January 2004

Charge-on-spring polarizable water models revisited: From water clusters to liquid water to ice

Haibo Yu
University of Wollongong, hyu@uow.edu.au

Wilfred van Gunsteren
ETH Zurich

Charge-on-spring polarizable water models revisited: From water clusters to liquid water to ice

Abstract

The properties of two improved versions of charge-on-spring ﬠCOSﬠ polarizable water models (COS/G2 and COS/G3) that explicitly include nonadditive polarization effects are reported. In COS models, the polarization is represented via a self-consistently induced dipole moment consisting of a pair of separated charges. A previous polarizable water model (COS/B2), upon which the improved versions are based, was developed by Yu, Hansson, and van Gunsteren ﬠJ. Chem. Phys. 118, 221 ﬠ2003ﬠﬠ. To improve the COS/B2 model, which overestimated the dielectric permittivity, one additional virtual atomic site was used to reproduce the water monomer quadrupole moments besides the water monomer dipole moment in the gas phase. The molecular polarizability, residing on the virtual atomic site, and Lennard-Jones parameters for oxygen-oxygen interactions were varied to reproduce the experimental values for the heat of vaporization and the density of liquid water at room temperature and pressure. The improved models were used to study the properties of liquid water at various thermodynamic states as well as gaseous water clusters and ice. Overall, good agreement is obtained between simulated properties and those derived from experiments and ab initio calculations. The COS/G2 and COS/G3 models may serve as simple, classical, rigid, polarizable water models for the study of organic solutes and biopolymers. Due to its simplicity, COS type of polarization can straightforwardly be used to introduce explicit polarization into (bio)molecular force fields.

Keywords

water, models, ice, liquid, charge, clusters, spring, revisited, polarizable, CMMB

Disciplines

Life Sciences | Physical Sciences and Mathematics | Social and Behavioral Sciences

Publication Details

Yu, H. & van Gunsteren, W. (2004). Charge-on-spring polarizable water models revisited: From water clusters to liquid water to ice. Journal of Chemical Physics, 121 (19), 9549.

Charge-on-spring polarizable water models revisited: From water clusters to liquid water to ice

Haibo Yu and Wilfred F. van Gunsteren*
Laboratory of Physical Chemistry, Swiss Federal Institute of Technology Zurich, ETH Hönggerberg, 8093 Zürich, Switzerland

(Received 15 June 2004; accepted 18 August 2004)

The properties of two improved versions of charge-on-spring (COS) polarizable water models (COS/G2 and COS/G3) that explicitly include nonadditive polarization effects are reported. In COS models, the polarization is represented via a self-consistently induced dipole moment consisting of a pair of separated charges. A previous polarizable water model (COS/B2), upon which the improved versions are based, was developed by Yu, Hansson, and van Gunsteren [J. Chem. Phys. **118**, 221 (2003)]. To improve the COS/B2 model, which overestimated the dielectric permittivity, one additional virtual atomic site was used to reproduce the water monomer quadrupole moments besides the water monomer dipole moment in the gas phase. The molecular polarizability, residing on the virtual atomic site, and Lennard-Jones parameters for oxygen-oxygen interactions were varied to reproduce the experimental values for the heat of vaporization and the density of liquid water at room temperature and pressure. The improved models were used to study the properties of liquid water at various thermodynamic states as well as gaseous water clusters and ice. Overall, good agreement is obtained between simulated properties and those derived from experiments and *ab initio* calculations. The COS/G2 and COS/G3 models may serve as simple, classical, rigid, polarizable water models for the study of organic solutes and biopolymers. Due to its simplicity, COS type of polarization can straightforwardly be used to introduce explicit polarization into (bio)molecular force fields. © *2004 American Institute of Physics*.
[DOI: 10.1063/1.1805516]

I. INTRODUCTION

Because of its biological importance and anomalous physical properties, water is by far the compound most studied with computer simulation. To obtain a molecular level understanding of physical and chemical phenomena of water,[1] an accurate interaction potential model is essential, and much effort has been directed towards the formulation of accurate models for water. Overviews of the historic development of water models have recently been presented by Wallqvist and Mountain,[2] Finney,[3] and Guillot.[4] Most (bio)molecular force fields,[5] such as AMBER/PARM94,[6] CHARMM27,[7] GROMOS 45A3,[8,9] and OPLS/AA,[10] used in computer simulations make use of simple pairwise potentials and include electronic many-body effects implicitly. Empirical (including rigid or flexible) water models[2] employed in (bio)molecular simulations, such as ST2,[11] SPC,[12] TIP3P, TIP4P,[13] SPC/E,[14] F3C,[15] TIP5P,[16,17] SPC/A,[18] SPC/L,[18,19] and SPC/S,[20] have provided considerable insights into the molecular origin of the unique behavior of water in various phases and its role as (bio)molecular solvent. These models use fixed partial charges and include many-body induced polarization in the condensed phase in an average, mean-field manner. The dipole moments of the various empirical water models are generally larger than the gas phase dipole (1.85 D) (Ref. 21) and vary between 2.1 D and 2.4 D (Ref. 4) [e.g., 2.27 D for SPC,[12] 2.35 D for TIP3P (Ref. 13)], in order to implicitly include polarization effects in liquid water. These models were usually parametrized to reproduce the experimental values for the heat of vaporization and density at ambient conditions. As a result, these nonpolarizable water models provide good descriptions of homogeneous bulk water. However, it is widely recognized that the use of fixed partial charges inhibits proper modeling of the molecular response to the molecular environment, especially for gas phase clusters, nonpolar solutes in polar solvents, and hydrogen-bonded liquids.[5,22–24] For example, the binding energy of a water dimer in the gas phase is overestimated by more than 20% in the SPC model.[12,25] In addition, water molecules in biomolecular systems encounter varying environments and the degree of polarization of individual water molecules will vary widely across a biomolecular system. The properties of water molecules in different environments are not properly modeled by nonpolarizable water models.

In response to this concern, a large number of polarizable water models has been developed, since the pioneering work by Vesely (1977),[26] Stillinger and David (1978),[27] Barnes *et al.* (1979),[28] and Warshel (1979)[29] more than 20 years ago. In literature, mainly three approaches have been explored to develop polarizable water models in the framework of classic mechanics: polarizable point dipole (PD), fluctuation charge (FQ), or Drude oscillator (DO) methods.[25,30–62] Polarizable water models have had considerable success in

*Author to whom correspondence should be addressed. Fax: 0041-1-632 1039; Electronic mail: wfvgn@igc.phys.chem.ethz.ch, igc-sec@igc.phys.chem.ethz.ch

extending the thermodynamic range of applicability of the water potential. Using these models heterogeneities and anisotropies near solid or gaseous interfaces, near ions or near biomolecules are more accurately described compared to when using nonpolarizable water models.[24] As early as 1977, the PD method has been used by Vesely[26] to develop polarizable models in which an induceable point dipole is placed on every polarizable center. Although being less successful in reproducing the dielectric permittivity of liquid water, the PD method correctly describes the polarizability effects in a variety of systems.[23] The main disadvantage of this method is the complex evaluation of dipole-dipole interactions and forces. In the FQ scheme, originating from the charge equilibration method,[39] the partial charges are dynamically varied in dependence of the local environment with the constraint of neutrality. As applied to water,[42] this model, though highly efficient, has the disadvantage that the polarizability is confined to the molecular plane, whereas experimentally the polarizability is nearly isotropic.[63] To overcome this drawback, combined PD and FQ models have been described.[53] The DO method[64] uses a harmonic restraining potential energy function to tether a mobile point charge of a fixed size to a particular interaction site. The DO method is essentially identical to the so-called shell model, which is often used in simulations of the solid state,[65] and both names are used in the literature.[24] One of the great practical advantages of the DO model is that all electrostatic interactions are point charge interactions. Thus it can very straightforwardly be combined with various methods of treating long-range interactions.[66–72]

Recently, we reported a simple, rigid, self-consistent polarizable water model (COS/B2) (Ref. 25) that was developed based on the charge-on-spring (COS) method.[35] In the COS approach, originating from the DO model, the induced dipole moment is represented by a pair of separated charges of fixed size. Their distance determines the induced dipole moment and only the first-order linear polarization effect is taken into account.[24] In the COS/B2 model one of the two charges resides on the oxygen atom and the displacement of the other charge (polarization charge) with respect to oxygen is determined in a combined predictive and iterative way, according to Eq. (2) in Ref. 25. The condensed phase properties of the COS/B2 model are in reasonable accord with experimental data.[25] The heat of vaporization, density, and dynamic properties of liquid water are well reproduced. Since the COS/B2 model was parametrized against the water properties in the liquid phase rather than those in the gas phase, the COS/B2 model has a dipole moment of 2.07 D, intermediate between the experimental gas phase dipole moment (1.85 D) (Ref. 21) and those of nonpolarizable water models and it fails to reproduce the proper optimal gas phase dimer structure, especially regarding the relative orientation of the two water monomers. In the liquid phase, the COS/B2 model does not show a pronounced structure beyond the first solvation shell in the oxygen-oxygen radial distribution function (RDF), which may relate to the fact that the COS/B2 model yields a less tetrahedrallike minimum-energy structure for the water dimer. Worst of all, the COS/B2 model overestimates the dielectric permittivity by 50% [$\epsilon(0)=122$], with an average molecular dipole moment of 2.62 D in the liquid phase at ambient conditions.

Sticking to the COS approach and in the framework of molecular mechanics, there are basically four possible ways to improve the COS/B2 model. First, Caldwell *et al.*[36] reported that the use of atom-centered polarizabilities rather than a molecular one appeared to lead to an improvement in their studies of liquids and ionic solutions. However, use of atom-centered polarizabilities instead of a molecular one will almost double the number of interaction sites in the model, which makes the computation rather expensive. Second, one may introduce molecular flexibility which has a sizeable effect on the properties of liquid water.[15,55,73–77] However, it has been shown that flexible water models are not superior to their rigid counterparts because of the difficulty to properly model the inherent quantum nature of stretching and bending vibrations in a classical way.[73] Third, one may introduce fixed point multipoles in addition to the monopole charges present at the atoms.[59,78] This would allow one to simultaneously reproduce both the dipole moment and the quadrupole moments of a water molecule.[36] This is not possible within an atom-centered three-point charge model. It has been noticed that using an atom-centered three-point charge model, in the liquid phase the oxygen-oxygen RDF shows little structure beyond the first peak,[25,46] which indicates that those types of models are not able to fully describe the tetrahedrallike water structure. In recent work by Ren and Ponder,[59] high-order point multipoles besides (monopole) partial charges were used to improve the description of the quadrupole moments. However, in commonly used (bio)molecular force fields,[5–10] only partial (monopole) charges are used to model the electrostatic interactions, and the introduction of higher-order pointmultipoles would make the computation complex and expensive. Fourth, a correct reproduction of the molecular dipole and quadrupole can also be reached by adding off-atom sites as in the TIP4P model.[50,51,53,55–58] This approach maintains the simplicity of the monopole-monopole interactions and at least partially the compatibility of the water model with current (bio)molecular force fields. Therefore, this approach is taken in this work. We will focus our effort on improving the performance of the COS water models by introducing a massless virtual-atom charge interaction site.

In the improved COS models, the polarization charge was kept at $-8.0e$, because it was shown in the previous paper[25] that the size of the polarization charge has fairly small effects on the properties of the COS water models, provided that the displacement of the polarization charge is small enough compared to the smallest nonbonded distance. The fixed partial charges on the hydrogen atoms and the position of the virtual atom site along the bisector of the HOH angle were chosen to reproduce both the molecular dipole and (approximately) quadrupole moments of the monomer in the gas phase. Keeping the simplicity of the models, a (one-center) molecular polarizability is used and the models are rigid. Our goal is to obtain a model with improved properties in the liquid phase compared to the nonpolarizable SPC water model and reasonable properties in the gas phase. The molecular polarizability and the oxygen-

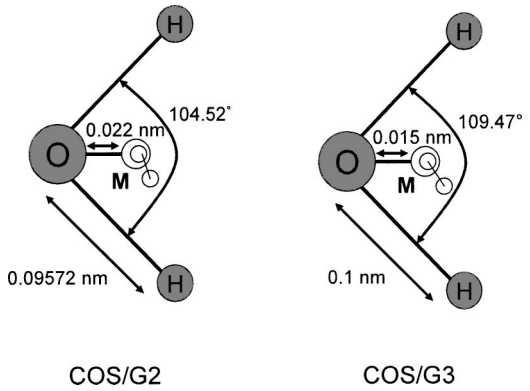

FIG. 1. Interaction sites and geometries of the COS/G2 and COS/G3 water models. The models consist of four Coulomb interaction sites located at the two hydrogen atoms, the virtual-atom site M, and the polarization charge, plus one van der Waals or Lennard-Jones site located at the oxygen atom. The HOH geometry is rigid while the polarization charge q_{pol} is connected by a spring to the M site which carries a charge $q_M - q_{pol}$ with $q_M = -2q_H$.

oxygen Lennard-Jones parameters were optimized to reproduce the heat of vaporization and density for liquid water at room temperature and pressure. Simulations of the improved water models over a wide range of temperatures and pressures in the liquid phase as well as of water clusters and ice were performed to further validate the range of applicability of the models.

This paper is organized as follows; Sec. II describes the method to develop the models and simulation details. Section III describes the results of the simulations, and Sec. IV presents conclusions and an outlook.

II. METHODS

A. Developing the model

As in the previous COS/B2 model, each water molecule has only one polarizable center. Different from the COS/B2 model, one additional virtual atomic center M was added at a fixed distance d_{OM} to the oxygen along the bisector of the HOH angle and the molecular polarizability resides on site M instead of at the oxygen atom (Fig. 1). Construction of the virtual atom site and distribution of the forces on the massless virtual atom over the other atoms are performed according to Ref. 79. The position of M, $\vec{r}_M$, is obtained according to Eq. (1):

$$\vec{r}_M = \vec{r}_O + \frac{\gamma}{2}(\vec{r}_{H_1O} + \vec{r}_{H_2O}) \tag{1}$$

where $\vec{r}_{H_1O} = \vec{r}_{H_1} - \vec{r}_O$, $\vec{r}_{H_2O} = \vec{r}_{H_2} - \vec{r}_O$, $\vec{r}_O$ is the position of the oxygen atom, $\vec{r}_{H_1}$ and $\vec{r}_{H_2}$ are the positions of the hydrogen atoms, and γ is a constant, which determines d_{OM} as a function of d_{OH}, the oxygen-hydrogen distance, and the HOH angle. The addition of the massless M site with the constraint applied [Eq. (1)] does not introduce any extra degrees of freedom into the molecule in the calculation of the

TABLE I. Parameters of the SPC, COS/B2, COS/G2, and COS/G3 water models. d_{OH}: OH bond length, ∠HOH: HOH bond angle, d_{OM}: OM distance, q_H: partial charge on the hydrogen, q_O: partial charge on the oxygen, q_M: partial charge on the M site, μ^0: (permanent) molecular dipole moment, Q_{xx}, Q_{yy}, Q_{zz}: quadrupole moment components, α_{xx}, α_{yy}, α_{zz}: molecular polarizability components, C6: attractive Lennard-Jones coefficient for oxygen-oxygen atoms, C12: repulsive Lennard-Jones coefficient for oxygen-oxygen atoms, and q_{pol}: polarization charge. The y and z axes lie in the plane of the molecule with the z axis along the C_2 axis of symmetry and the origin is put at the center of mass. The values for the quadrupole moments of the various water models reported in Ref. 46 were computed with putting the origin at the oxygen atom of the water molecule, while the experimental data were determined by putting the origin at the center of mass of the water molecule.

Model	SPC[a]	COS/B2[b]	COS/G2	COS/G3	Expt.	*Ab initio*
Number of force centers	3	4	5	5		
d_{OH} (nm)	0.10000	0.10000	0.09572	0.10000	0.09572±0.0003 (gas)[c] 0.09700±0.0005 (liquid)[e]	0.0972 (gas)[d] 0.0991 (liquid)[d]
∠HOH (deg)	109.47	109.47	104.52	109.47	104.52±0.05 (gas)[c] 106.1±1.8 (liquid)[e]	104.4 (gas)[d] 105.5 (liquid)[d]
d_{OM} (nm)	0.00	0.00	0.022	0.015		
q_H (e)	0.410	0.373	0.5265	0.450672		
q_O (e)	−0.820	−0.746	0	0		
q_M (e)	⋯	⋯	−1.0530	−0.901344		
μ^0 (D)	2.27	2.07	1.85	1.85	1.855[f]	1.840[g]
Q_{zz} (10^{-1} D nm)	−1.82	−1.66	−2.07	−1.99	−2.50[h]	−2.42[g]
Q_{yy} (10^{-1} D nm)	2.11	1.93	2.27	2.33	2.63[h]	2.57[g]
Q_{xx} (10^{-1} D nm)	−0.29	−0.27	−0.20	−0.34	−0.13[h]	−0.14[g]
α_{zz} (10^{-2} nm^3)	⋯	0.0930	0.1255	0.1250	0.1415[i]	0.138[g]
α_{yy} (10^{-2} nm^3)	⋯	0.0930	0.1255	0.1250	0.1528[i]	0.147[g]
α_{zz} (10^{-2} nm^3)	⋯	0.0930	0.1255	0.1250	0.1468[i]	0.142[g]
C6 (10^{-3} kJ mol^{-1} nm^6)	2.61735	2.75691	3.24434	3.86709		
C12 (10^{-6} kJ mol^{-1} nm^{12})	2.63413	3.01500	3.45765	3.95831		
q_{pol} (e)	⋯	−8.0	−8.0	−8.0		

[a]Reference 12.
[b]Reference 25.
[c]Reference 134.
[d]Reference 102.
[e]Reference 135.
[f]Reference 24.
[g]Reference 130.
[h]Reference 136.
[j]Reference 63.

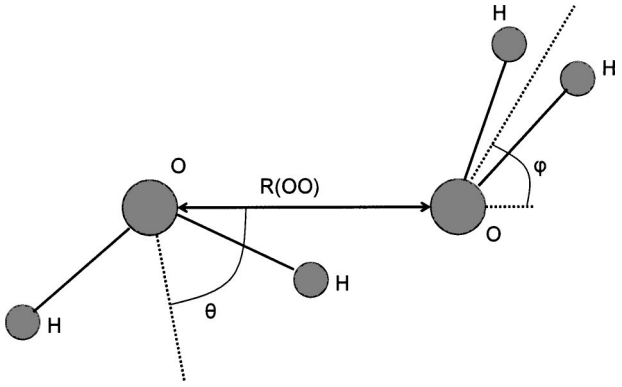

FIG. 2. Definition of the distance $R(\mathrm{OO})$ and the angles θ and ϕ that determine the relative position and orientation of the monomers of the water dimer in the gas phase.

kinetic energy of the system. The "pseudoforce" $\vec{f}_M$ that acts on the virtual-atom site M should be redistributed according to Eq. (2):

$$\vec{F}_{\mathrm{H}_1}=\vec{f}_{\mathrm{H}_1}+\frac{\gamma}{2}\vec{f}_M\,,$$

$$\vec{F}_{\mathrm{H}_2}=\vec{f}_{\mathrm{H}_2}+\frac{\gamma}{2}\vec{f}_M\,, \tag{2}$$

$$\vec{F}_{\mathrm{O}}=\vec{f}_{\mathrm{O}}+(1-\gamma)\vec{f}_M\,.$$

The OH bond lengths and HOH bond angles are set to either the experimental gas phase values (model COS/G2: 0.095 72 nm and 104.52°) or the SPC-type ideal tetrahedral structure values (model COS/G3: 0.100 00 nm and 109.47°). The geometries of the models are depicted in Fig. 1. The distance d_{OM} (or the constant γ) and charges q_{H} were chosen to reproduce both the gas phase molecular dipole moment and (approximately) quadrupole moments. Generally, there are two ways to parametrize an empirical model: calibration against gas phase results from high-level *ab initio* calculations[80] or parametrizing against the experimental (thermodynamic) properties of liquid water. In our work, the latter approach is taken as was done in the GROMOS force field.[8,81,82] According to *ab initio* calculations by Morita and Kato,[83,84] the molecular polarizability of water in the condensed phase can be 18% lower than in the gas phase. In addition, Stern *et al.*[53] concluded from their work on polarizable force fields that Pauli exclusion effects should reduce

TABLE II. Optimal (minimum energy) geometry, interaction energy U^{pot}, total dipole moment μ^{dimer}, and average molecular dipole moment μ^{mean} of the gas phase dimer for the COS/B2, COS/G2, and COS/G3 models, for various models reported in literature and values from experiments and *ab initio* calculations. The dimer geometry is defined by the O–O distance $R(\mathrm{OO})$, with angles θ and ϕ as defined in Fig. 2. The water monomer quadrupole moment components (see Table I caption for definition) are listed for comparison. The experimental interaction energy was obtained after vibration correction of the experimental association energy at 373 K (Ref. 132). The experimental structural and dielectric properties were obtained by molecular beam microwave spectroscopy at 20 K (Ref. 133).

Model	$R(\mathrm{OO})_{\min}$ (nm)	$\theta_{\min}$ (deg)	$\phi_{\min}$ (deg)	U^{pot} (kJ mol^{-1})	μ^{dimer} (D)	μ^{mean} (D)	Q_{xx} (10^{-1} D nm)	Q_{yy} (10^{-1} D nm)	Q_{zz} (10^{-1} D nm)
Expt.[a]	0.295	51±10	57±10	−22.6±2.5	2.60		−2.50	2.63	−0.13
Ab initio[b]	0.291	56	58	−21.00	2.68	2.10	−2.42	2.57	−0.14
SPC[c]	0.275	52	23	−27.65	3.59	2.27	−1.82	2.11	−0.29
TIP3P[d]	0.273	52	27	−27.20			−1.68	1.76	−0.08
TIP4P[d]	0.274	54	50	−26.35	2.70		−2.09	2.20	−0.11
SPC/E[e]	0.274	52	22	−30.10	3.76	2.35	−1.88	2.19	−0.30
TIP5P[f]	0.268	51	50	−28.37	2.92	2.29	−1.48	1.65	−0.17
COS/B2[g]	0.279	51	20	−23.29	3.76	2.26	−1.66	1.93	−0.27
COS/G2	0.281	56	74	−20.90	2.08	2.03	−2.07	2.27	−0.20
COS/G3	0.287	56	50	−20.50	2.71	2.04	−1.99	2.33	−0.34
TIP4P-FQ[h]	0.292	52	27	−18.82	3.43	2.06	−1.79	1.88	−0.10
PPC[i]	0.281	51	26	−24.10			−1.92	2.06	−0.15
TIP4P-pol-3[j]	0.277	55	40	−22.20		2.07	−1.79	1.88	−0.10
SWFLEX-AI[k]	0.295	56	55	−21.78	2.59		−2.50	2.63	−0.13
SWFLEX-ISO[k]	0.295	54	57	−21.75	2.65		−2.50	2.63	−0.13
SWRIGID-AI[k]	0.294	59	59	−21.91	2.55		−2.50	2.63	−0.13
SWRIGID-ISO[k]	0.293	57	56	−21.91	2.47		−2.50	2.63	−0.13
MCDHO[l]	0.292	57	56	−20.90	2.68	2.09	−2.44	2.67	−0.24
POL5/TZ[m]	0.290	57	63	−20.75	2.43	2.06	−2.34	2.34	0.00
POL5/QZ[m]	0.290	57	62	−20.75	2.44	2.06	−2.34	2.34	0.00
AMOEBA[n]	0.289	58	57	−20.75	2.54	2.02	−2.17	2.50	−0.33
SWM4-DP[o]	0.282		70	−21.95	2.09		−2.16	2.41	−0.24

[a]References 132, 133, and 136.
[b]References 90, 130, 137, and 138.
[c]Reference 12.
[d]Reference 13.
[e]Reference 14.
[f]Reference 16.
[g]Reference 25.
[h]Reference 42.
[i]Reference 45.
[g]Reference 51.
[k]Reference 55.
[l]Reference 139.
[m]Reference 53.
[n]Reference 59.
[o]Reference 60.

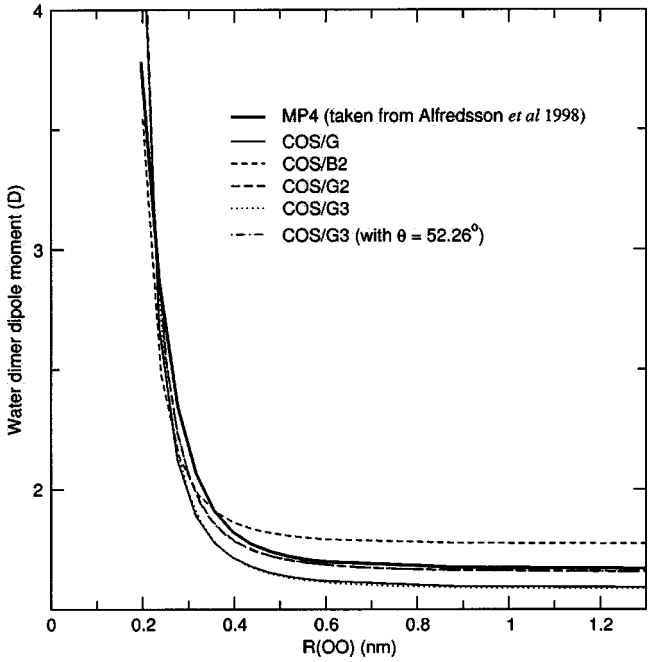

FIG. 3. Total dipole moment of the water dimer as a function of $R(\mathrm{OO})$ distance for water models together with that from the restricted Hartree-Fock MP4 calculations by Alfredsson *et al*. (Ref. 93). The dimer geometry was set to COS/G2: $\theta=52.26°$, COS/G3, COS/G, COS/B2: $\theta=54.74°$ and $\phi=74.6°$, if not specified otherwise. MP4: thick solid line, COS/G: solid line, COS/B2: short-dashed line, COS/G2: dashed line, COS/G3: dotted line, and COS/G3 (with $\theta=52.26°$): dotted-dashed line.

the effective polarizability of water molecules in the condensed phase compared to the gas phase. In our parametrization, the molecular polarizability was treated as an empirical parameter and allowed to vary. Additionally, the oxygen-oxygen Lennard-Jones parameters were optimized to best reproduce the heat of vaporization and density of liquid water at room temperature and pressure. The final sets of parameters for the COS/G2 and COS/G3 models together with those for the SPC and COS/B2 models are listed in Table I.

B. Simulation methods

A cubic box with a side length of 3.107 nm was filled with 1000 water molecules, resulting in a density of 997.0 $\mathrm{kg\,m^{-3}}$, which is the experimental value of liquid water at 298 K and 1 atm.[85] Molecular dynamics simulations were performed under *NPT* or *NVT* conditions with the GROMOS96 (Groningen molecular simulation) package,[8,86] modified to incorporate the polarizable model. The geometries of the water molecules were constrained by applying the SHAKE (Ref. 87) algorithm with a relative geometric tolerance of 10^{-4}. The temperature was weakly coupled to a bath of a given temperature with a relaxation time of 0.1 ps (Ref. 88) and in the *NPT* simulations the pressure was also weakly coupled to a bath of a given pressure with a relaxation time of 0.5 ps,[88] for which the compressibility of the system was set to the experimental value at 298 K and 1 atm of $7.513\times10^{-4}\,(\mathrm{kJ\,mol^{-1}\,nm^{-3}})^{-1}$.[85] This choice of temperature and pressure coupling together with the quoted parameter values has been shown to have a negligible effect on the dynamic properties of liquid water.[88] The equations of motion were integrated using the leap-frog algorithm with a time step of 2 fs. Triple-range cutoff radii of 0.8/1.4 nm were used to treat van der Waals and electrostatic interactions, where the intermediate range interactions were calculated, concurrently to updating the pairlist for short range interactions, every fifth time step. The interactions between atom pairs within the shorter cutoff were calculated every time step. The long range electrostatic interactions beyond the outer cutoff were represented by a reaction field[66,68] with $\epsilon_{RF}=78.5$. At the beginning of the simulation, the velocities of the atoms were assigned from a Maxwell distribution at a given temperature. For every water model, 100 ps of equilibration was followed by 500 ps simulation used for the calculation of the various properties. During the runs, configurations of the system were saved every 0.5 ps. The static dielectric permittivity $\epsilon(0)$ was computed in the *NPT* ensemble from 10 separate independent runs of 400 ps each to ensure the convergence.

The starting structure of ice Ih was taken from the $3\times2\times2$ unit cell with 96 water molecules constructed by Hayward and Reimers.[89] This unit cell contains 12 ($3\times2\times2$) copies of the smallest unit cell for ice Ih, which contains eight water molecules. The $3\times2\times2$ unit cell was copied three times along each of the x, y, and z axes to ensure a big enough box for the triple-range cutoff, resulting in a box with side lengths of 4.056, 4.684, and 4.416 nm. The structure was equilibrated first by *NVT* simulation periods (each 5 ps long) with the temperature increasing from 1 K to 50 K and then by *NPT* simulation periods (each 5 ps long) under isotropic pressure coupling with the temperature increasing from 50 K to 100 K. Then simulation was performed at 100 K under isotropic pressure (1 atm) coupling for 500 ps.

C. Analysis

For each model that was found to reproduce reasonably well the experimental density and heat of vaporization, a variety of structural, thermodynamic, dynamic, and electrostatic properties were further evaluated, partly as function of temperature and pressure. See Ref. 25 for details.

III. RESULTS AND DISCUSSION

A. Gas phase water

A comparison of the molecular dipole moment, quadrupole moments, and polarizability of a single isolated water molecule calculated for the SPC, COS/B2, COS/G2, COS/G3 models with the experimental and *ab initio* values is given in Table I. The dipole moments of the SPC model (2.27 D) and the COS/B2 model (2.07 D) are larger than the experimental gas phase dipole moment (1.855 D) (Ref. 21) to include prepolarization in order to better reproduce the properties in the liquid phase. The COS/G2 and COS/G3 models reproduce the molecular dipole moment exactly and the quadrupole moments approximately. These models are rigid models with a geometry closer to the experimental geometry either in the gas phase (COS/G2) or in the liquid phase (COS/G3).

TABLE III. Water cluster minimum-energy properties: interaction energy U (kJ/mol), polarization energy U^{pol} (kJ/mol), average distance between oxygens in hydrogen bonds R_{OO} (nm), total molecular dipole moment μ_{tot} (D), and average molecular dipole moment μ (D). The optimal cluster conformations for the COS/G2 model are shown in Fig. 4.

		COS/G2	COS/G3	*Ab initio*	Expt.
Trimer	U (kJ mol^{-1})	−55.9	−54.8	−61.9,[a] −62.1,[b] −59.6,[c] −66.1[d]	
Cyclic	U^{pol} (kJ mol^{-1})	9.1	9.1		
	R_{OO} (nm)	0.294	0.295	0.279,[e] 0.283,[a], 0.280,[b] 0.278[f]	0.296,[g] 0.285[h]
	μ (D)	2.14	2.13	2.31[i]	
	μ_{tot} (D)	1.10	1.10	1.14,[e] 1.071[i]	
Tetramer	U (kJ mol^{-1})	−103.4	−101.1	−115.48,[d] −99.6,[b] −106.0[c]	
Cyclic	U^{pol} (kJ mol^{-1})	30.8	31.8		
	R_{OO} (nm)	0.286	0.286	0.274[e]	0.279[h]
	μ (D)	2.40	2.34	2.56[i]	
	μ_{tot} (D)	0.01	0.01	0.00[e]	
Pentamer	U (kJ mol^{-1})	−136.4	−134.1	−151.9,[d] −139.5[c]	
Cyclic	U^{pol} (kJ mol^{-1})	55.5	58.5		
	R_{OO} (nm)	0.283	0.283	0.272,[e] 0.287[b]	0.277[h]
	μ (D)	2.45	2.47	2.67[i]	
	μ_{tot} (D)	0.94	0.94	1.04,[e] 0.927[i]	
Hexamer	U (kJ mol^{-1})	−172.1	−166.4	−190.8,[d] −187.2[j]	
Book	U^{pol} (kJ mol^{-1})	62.1	67.8		
	R_{OO} (nm)	0.280	0.270	0.277,[e] 0.277[j]	
	μ (D)	2.43	2.45		
	μ_{tot} (D)	2.11	2.12	2.49[e]	
Hexamer	U (kJ mol^{-1})	−173.4	−170.3	−191.6,[d] −188.4[j]	
cage	U^{pol} (kJ mol^{-1})	43.6	44.0		
	R_{OO} (nm)	0.286	0.281	0.281,[e] 0.281[j]	0.282[h]
	μ (D)	2.34	2.34	2.64[i]	
	μ_{tot} (D)	1.99	2.00	2.01[e]	1.90[k]
Hexamer	U (kJ mol^{-1})	−167.4	−160.7	−187.5,[d] −183.6[d]	
Cyclic	U^{pot} (kJ mol^{-1})	81.9	90.3		
	R_{OO} (nm)	0.269	0.267	0.271,[e] 0.271[j]	0.276[h]
	μ (D)	2.53	2.56	2.70[i]	
	μ_{tot} (D)	0.04	0.04	0.00[e]	
Hexamer	U (kJ mol^{-1})	−172.2	−167.4	−192.1,[d] −188.8[d]	
Prism	U^{pol} (kJ mol^{-1})	46.1	45.8		
	R_{OO} (nm)	0.287	0.287	0.284,[e] 0.284[j]	
	μ (D)	2.36	2.36		
	μ_{tot} (D)	2.58	2.61	2.77[e]	

[a]Reference 140.
[b]Reference 141.
[c]Reference 142.
[d]Reference 96.
[e]Reference 138.
[f]Reference 143.
[g]References 144 and 145.
[h]Reference 146.
[i]Reference 137.
[j]Reference 147.
[k]References 137 and 146.

The optimal dimer geometry in the gas phase was obtained by varing the relative position and orientation of the two molecules as given by the variables $R(OO)$, θ, and ϕ (as sketched in Fig. 2), and performing a global conformational search. The minimum-energy structures of the COS/G2 and COS/G3 water dimers are compared with experimental data and *ab initio* results in Table II. Results for other water models reported in literature are also listed for comparison. For the water dimer the *ab initio* results are more reliable than the experimental data. Correction of the experimentally determined association energy in hot vapor and the structure derived from microwave spectroscopy for anharmonic vibration and temperature effects is problematic.[90] The previous model COS/B2 improved the binding energy of the water dimer compared to the SPC model with a very "flat" (low ϕ value) optimal dimer geometry. This is essentially due to the lack of lone pairs in the model.[24] The COS/G2 and COS/G3 dimer results are in agreement with the corresponding *ab initio* values. The angle ϕ in the COS/G2 dimer is larger than the experimental one, as observed for the POL5/TZ, POL5/QZ, and SWM4-DP models. Coulson and Eisenberg[91] have shown that in ice over 20% of the total value of the interaction energy is contributed by the quadrupole moments. It has also been shown that both the dipole and quadrupole moments play a critical role in simulating hydrogen-bond strength and directionality of polar molecules.[92] An atom-centered three-point charge model can not reproduce both the dipole and the quadrupole moments of a water molecule at the same time.[25,36] We were unable to parametrize a three-point charge model for liquid water using the charges that reproduce the water dipole in the gas phase.[25] As we can see from various nonpolarizable and polarizable water models, only those models that reproduce the quadrupole moments fairly well produce a correct optimal dimer geometry in the gas phase either by introducing multipole moments[59] or by using off-atom virtual sites.[50,51,53,55–58] The total dimer di-

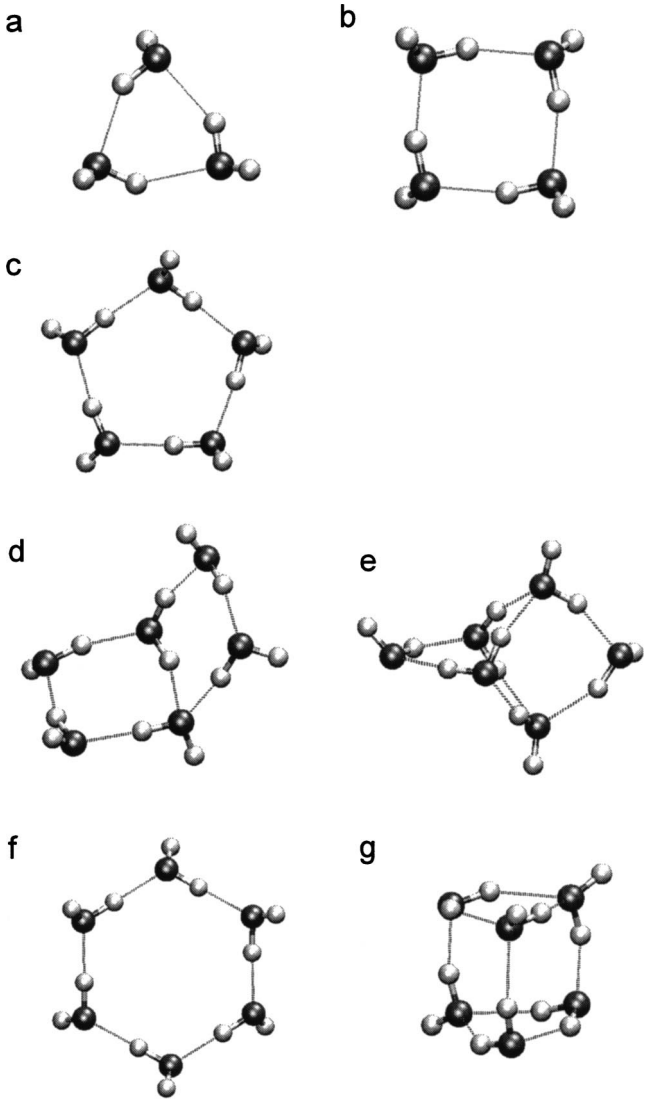

FIG. 4. Optimal structure of water clusters [(a) trimer, (b) tetramer, (c) pentamer, (d) book hexamer, (e) cage hexamer, (f) cyclic hexamer, (g) prism hexamer] of the model COS/G2. The structures are obtained from an energy minimization starting from the structure optimized by MP2/aug-cc-pVTZ calculations. See Table III for the structural details.

pole moment strongly depends on the orientation of the two monomers. Thus only those models that reproduce the optimal orientation will reproduce the total dipole moment of the water dimer. Additionally, the out-of-plane polarizability does also have a large effect on the optimal dimer structure. The models that fail to model the out-of-plane polarizability, for example, the models TIP4P/FQ (Ref. 42) and PPC,[45] cannot reproduce the tetrahedrallike structure of the water dimer.[31,56] Only by adding polarizable point dipoles to the FQ model, the POL5/TZ and POL5/QZ models were able to reproduce the optimal dimer geometry very well.[53] Generally, in order to obtain a model yielding the correct optimal dimer structure, the quadrupole moments and the out-of-plane polarizability should be properly modeled.

The total dipole moment of the water dimer as a function of the oxygen-oxygen distance, $R(\mathrm{OO})$, for the COS/G2 and COS/G3 models is shown in Fig. 3 together with that from the restricted Hartree-Fock Fourth order Møller-Plesset perturbation theory (MP4) calculations by Alfredsson *et al.*[93] In the calculations, the dimer geometry was fixed with $\phi=74.6°$ and $\theta=52.26°$ (COS/G2) or $\theta=54.74°$ (COS/G3). The θ values are such that the oxygen atom and one hydrogen atom from the hydrogen-bond donor molecule and the oxygen atom from the acceptor molecule are on a line. The COS/G2 model reproduces the total dipole moment of the water dimer better than the COS/G3 model. However, we notice that the intramolecular geometry of the COS/G3 model is slightly different from the geometry used in MP4 calculations. By changing the angle θ from 54.74° to 52.26°, the COS/G3 model reproduces the MP4 results better. Only at distances $R(\mathrm{OO})$ shorter than 0.24 nm, the dipole moment is overestimated by both models. Such distances are rarely observed in the simulation of liquid water at ambient pressures as we can see from the radial distribution functions of liquid water (see Sec. III B). For this reason, no Thole-like[94] damping factors had to be used to decrease the polarization effect at short distance as done in the models of Refs. 50 and 57–59.

Following the calculations of Stern *et al.*,[53] we have investigated the cyclic trimer, tetramer, and pentamer, as well as book, cage, cyclic, and prism configurations of the hexamer using the COS/G2 and COS/G3 models. The binding energies, average O–O distances, average molecular dipole moments, and total dipole moments of the clusters for various models are listed in Table III. In accordance with Stern *et al.*,[53] we did not perform a global conformational search, but started from *ab initio* minimized geometries and performed an energy minimization with the model potentials. The *ab initio* calculations were performed at MP2/aug-cc-pVTZ level using the GAUSSIAN 98 package.[95] Structures for the various clusters as given by the COS/G2 model are shown in Fig. 4. Only recently, MP2 calculations for the water clusters with complete basis set limit estimation became available.[96] Generally, the binding energies of the water clusters are close to the less negative values from the *ab initio* calculations, which may be due to the fact that the models have a lower molecular polarizability compared to the experimental value in the gas phase.[63] The water hexamer represents a crossover point, where noncyclic structures become more stable than the cyclic one. The COS/G2 and COS/G3 models predict correctly the relative stability of the case, book, and cyclic hexamers, but fail to predict the larger stability of the prism with respect to the cage hexamer cluster. However, the difference in binding energy between these clusters is very small (less than 2%) and there does exist uncertainty in both experimental and *ab initio* data[97] as we can see from the recent review by Keutsch *et al.*[98] on the water trimer. It should also be kept in mind that in the *ab initio* calculations the intramolecular geometries were allowed to relax while in the calculations with the COS/G2 and COS/G3 models the intramolecular geometries were kept rigid. Notwithstanding, the predicted geometries are generally in good agreement with the experimental data and *ab initio* results. Taking into account the fact that the COS/G2 and COS/G3 models were parametrized against the properties of liquid water instead of gas-phase properties from *ab initio* calculations, both models describe the properties of the gaseous clusters rather well. The variation of the

TABLE IV. Liquid state properties of water at 1 atm and 300 K. Temperature T, pressure p, total potential energy U^{pot}, polarization energy U^{pol}, density ρ, self-diffusion constant D, rotational relaxation times along different axes τ_2^{HH}, τ_2^{OH}, and τ_2^{μ}, average (total and induced) molecular dipole μ and μ_{ind}, static dielectric permittivity $\epsilon(0)$, infinite frequency dielectric permittivity $\epsilon(\infty)$, infinite system Kirkwood factor g_k, Debye dielectric relaxation time τ_D, heat capacity C_p, isothermal compressibility κ_T, and thermal expansion coefficient α.

	SPC[12,25]	COS/B2[25]	COS/G2	COS/G3	*Ab initio*	Expt.
T (K)	302.4	302.5	302.8	302.0		300
P (atm)	−0.28	5.50	0.93	0.10		1
U^{pot} (kJ mol^{-1})	−41.26	−41.73	−41.30	−41.10		−41.5[a]
U^{pot} (kg mol^{-1})	⋯	11.54	15.40	14.38		
ρ (kJ m^{-3})	970.5	992.4	997.2	1000.0		997.0[b]
D 10^{-9} (m^2 s^{-1})	4.3	2.6	2.3	2.6		2.3[c]
τ_2^{HH} (ps)	1.1	1.7	2.4	1.7		2.0[d]
τ_2^{OH} (ps)	1.0	1.6	2.2	1.6		1.95[e]
τ_2^{μ} (ps)	0.9	1.6	2.0	1.4		1.92[f]
μ (D)	2.27	2.62	2.59	2.57	2.06,[g] 2.95–3.00[h]	2.9±0.6[i]
μ_{ind} (D)	⋯	0.58	0.78	0.75	∼0.81,[g] ∼1.08[h]	∼0.75,[j] ∼1.24[k]
$\epsilon(0)$	65.2	121.6	87.8	88.1		78.5[l]
$\epsilon(\infty)$	2.45	2.67	3.18	2.12		1.79,[m] 5.2[n]
g_k	2.57	3.55	2.53	2.70		2.90[o]
τ_D (ps)	6.8	14.9	9.9	9.2		8.3[p]
C_P (J mol^{-1} K^{-1})	75.9	88.1	94.1	83.7		75.32[q]
k_T 10^{-6} (atm^{-1})	47.3	46.4	40.8	39.5		45.8[q]
α 10^{-4} (K^{-1})	7.3	9.7	5.7	7.0		2.57[q]

[a]Reference 121.
[b]Reference 85.
[c]Reference 148.
[d]Reference 149.
[e]Reference 150.
[f]Reference 151.
[g]Reference 105.
[h]Reference 102.
[i]Reference 108.
[j]Reference 91.
[k]Reference 103.
[l]Reference 100.
[m]Reference 111.
[n]Reference 112.
[o]Reference 152.
[p]Reference 112.
[q]References 85 and 100.

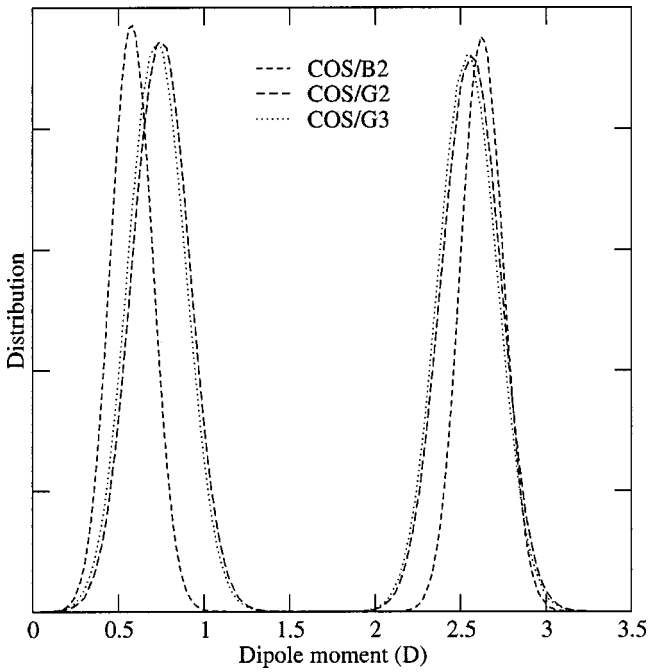

FIG. 5. Distribution of the induced dipole moment (left peaks) and the total dipole moment (right peaks) in the simulations of the COS/B2 (short-dashed line), COS/G2 (dashed-line), and COS/G3 (dotted line) models at room temperature and pressure.

average molecular dipole moment and the polarization energy between various water clusters illustrates the variation of many-body effects with the environment. Nonpolarizable water models will not capture these variations.

B. Liquid water at room temperature and pressure

Thermodynamic, dynamic, and dielectric properties of the COS/G2 and COS/G3 models for liquid water at room temperature and pressure are reported in Table IV together with the data for the SPC model, the COS/B2 model, and data available from experiments and *ab initio* calculations. The models were parametrized to fit to the experimental density and heat vaporization, so they reproduce them very well. The polarization energy was calculated from $U^{pol} = \frac{1}{2}\Sigma_{i=1}^{N}(\vec{\mu}_i^{ind} \cdot \vec{\mu}_i^{ind})/\alpha_i$, corresponding to the energy cost of distorting the molecule to its polarized state.[14] The polarization energy accounts for about 35% of the potential energy, a value comparable to the values found for different water clusters (see Table III). In nonpolarizable water models, this contribution is usually included implicitly in a mean-field manner via parametrization.

The dynamic properties of liquid water are likely to be correlated with the average molecular dipole moment.[33,99] The coupling between the translational motion and the dipole moment is indicated in the dielectric spectrum.[42] For ex-

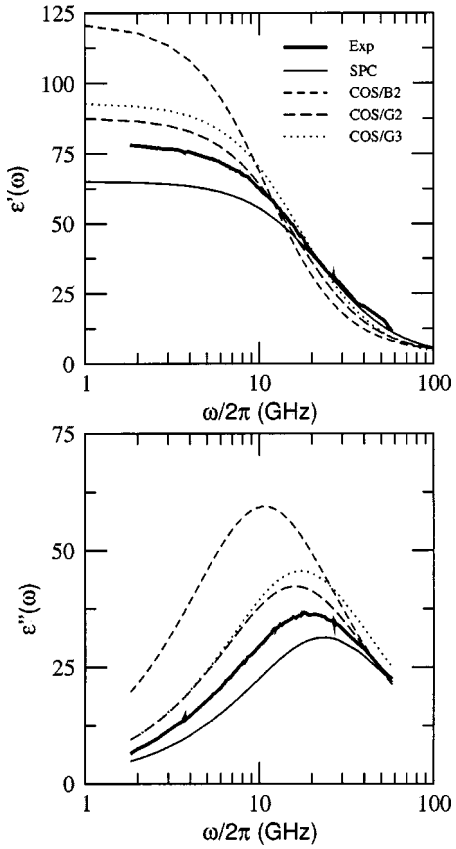

FIG. 6. The frequency dependence of the dielectric permittivity [real part $\epsilon'(\omega)$ and negative imaginary part $\epsilon''(\omega)$] at room temperature and pressure for the different water models. Experimental data (Ref. 112): thick line, SPC: solid line, COS/B2: short-dashed line, COS/G2: dashed line, and COS/G3: dotted line.

ample, the SPC model has a too high diffusion constant and a too fast orientational relaxation,[18,19] which is due to the fact that the SPC model has a too small dipole moment in the liquid phase. In contrast, the self-diffusion constant and the rotational relaxation times along different axes are well reproduced by the COS/B2, COS/G2, and COS/G3 models (Table IV).

The static dielectric permittivities $\epsilon(0)$ of liquid water at room temperature are about 88 (Table IV) for the COS/G2 and COS/G3 models, in satisfactory agreement with the experimental value of 78.5.[100] By introducing an off-atom interaction site to better reproduce the quadrupole moments, the COS/G2 and COS/G3 models do improve the static dielectric permittivity, which is one of the main deficiencies of our previous model COS/B2.[25] The COS/G2 and COS/G3 models give average molecular dipole moments of 2.59 D and 2.57 D in the liquid, about 40% larger than in the gas phase. The larger value in the liquid is a direct effect of polarization. The distribution of the total molecular dipole moment is nearly Gaussian with a width at half-height of $\approx$0.4 D for both cases (shown in Fig. 5), which is much smaller than that of the AMOEBA model (0.8 D).[59] The "correct" value of the average molecular dipole moment of liquid water is still in debate.[53,54,101,102] The dipole moment cannot be measured directly in experiments, nor can it be defined unambiguously, since the electron density is not zero between molecules.[103,104] Calculation of the average molecular dipole moment from *ab initio* simulations of liquid water suffers from the ambiguity in partitioning the electron density.[102,105,106] The average molecular dipole moments of reported polarizable water models vary between 2.3–3.1 D.[4] A wide range of values was also reported in the literature for liquid water and ice either from experiments or *ab initio* calculations: 2.6 D for ice Ih experimentally by Coulson and Eisenberg,[91] 3.09 D for ice Ih experimentally by Batista *et al.*,[103] 2.3–3.1 D for ice Ih from *ab initio* calculations by Batista *et al.*,[107] 2.66 D for liquid water from *ab initio* calculations by Laasonen *et al.*,[105] 2.95–3.00 D for liquid water from *ab initio* calculations by Silvestrelli and Parrinello,[102] and 2.9±0.6 D for liquid water extracted from an x-ray structure by Badyal *et al.*[108] Sprik[101] suggested that a polarizable water model needs an average dipole moment of 2.6 D to reproduce the static dielectric permittivity using classical molecular dynamics simulations and this conjecture has been confirmed by Soetens *et al.*[109] through analysis of a series of polarizable water models. Chen *et al.*[51] inferred from their studies on polarizable water models that an average dipole moment of about 2.4–2.5 D for a SPC-pol or TIP4P-pol model would yield a static dielectric permittivity around 80. On the other hand, polarizable models with dipole moments larger than 2.6 D and static dielectric permittivity around 80 have been reported.[54,59] Thus it is very risky to make any definitive conclusions on the relation between the molecular dipole moment and the static dielectric permittivity based on our results. The induced dipole moments of the COS/G2 and COS/G3 models are 0.78 and 0.75 D, which are larger than that of the COS/B2 model. They are closer to 0.75 D, the lower limit estimated from Coulson and Eisenberg's data,[91] than to 1.24 D from data of Batista *et al.*[103] A wide range of values for the induced dipole moment have been reported from *ab initio* or combined QM/MM calculations.[102,105,110] Compared to the COS/B2 model, the COS/G2 and COS/G3 models improve the infinite system Kirkwood factor g_K. The Debye dielectric relaxation time τ_D gives an estimate of the relaxation time of the hydrogen bond network and we expect that the COS/G2 and COS/G3 models mimic the hydrogen bond network more properly than the COS/B2 model. The frequency dependent dielectric permittivity [both the real part $\epsilon'(\omega)$ and the negative imaginary part $\epsilon''(\omega)$] is shown in Fig. 6. In the high-frequency range, the results are not reliable because of the sampling rate used in our simulations. The real part $\epsilon'(\omega)$ is at low frequency mainly determined by the static dielectric permittivity $\epsilon(0)$, while in the intermediate frequency range, it is mainly determined by the Debye relaxation time τ_D. The infinite frequency dielectric permittivity $\epsilon(\infty)$ of the COS/G2 and COS/G3 models are 3.18 and 2.12, which are within the range of the experimental data.[111,112] The COS/G2 and COS/G3 models improve the imaginary part $\epsilon''(\omega)$ compared to the COS/B2 model.

The heat capacity C_p, thermal expansion coefficient α, and isothermal compressibility κ_T at 1 atm and 298 K were evaluated using a finite difference expression as done in Ref. 25. The heat capacity $C_p=(\partial U/\partial T)_p$ was calculated using a centered-difference approximation instead of using the fluctuation formula in order to get more reliable results.[113] Gen-

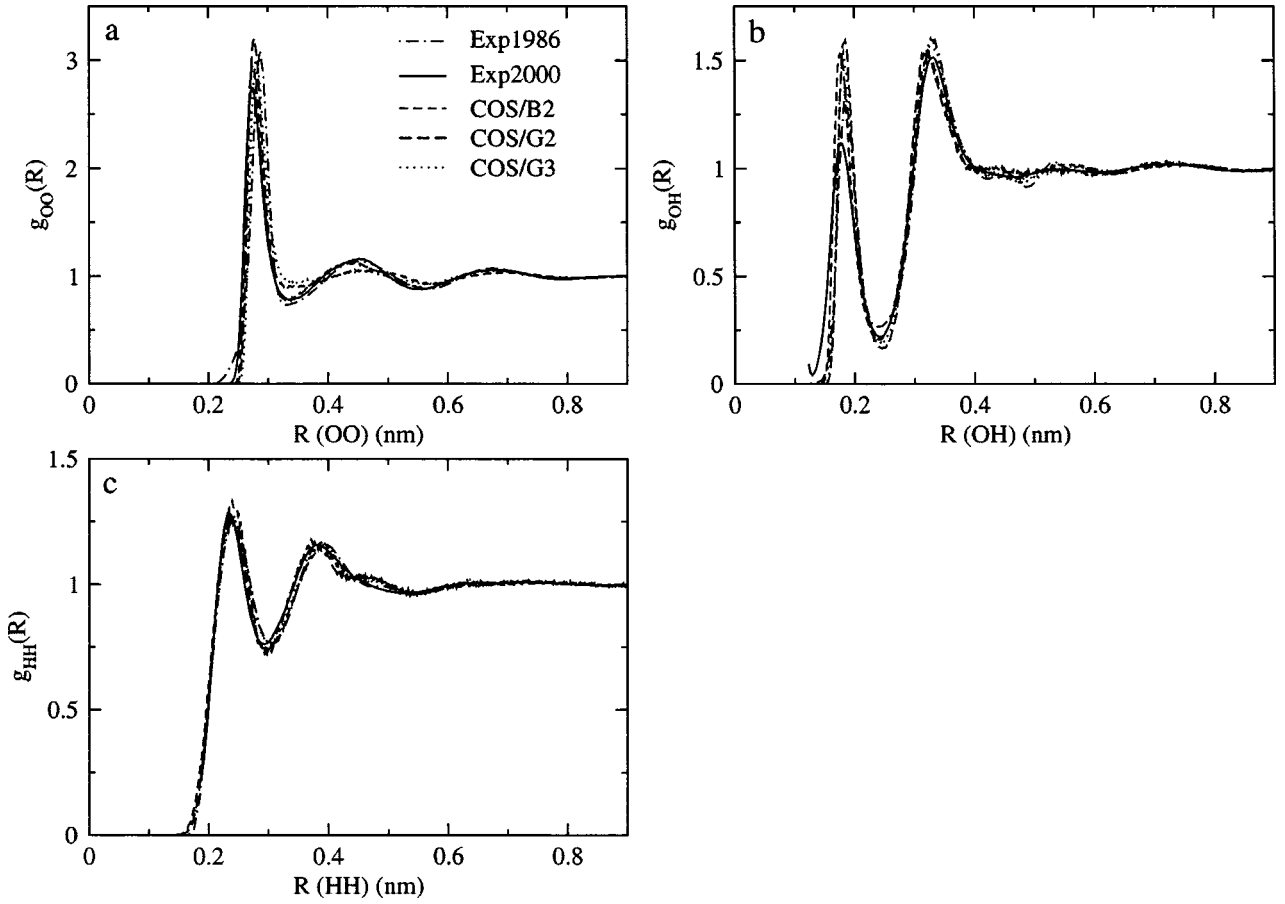

FIG. 7. Liquid phase atom-atom radial distribution function at room temperature and pressure for oxygen-oxygen (a), oxygen-hydrogen (b), and hydrogen-hydrogen (c) pairs for the set of water models, COS/B2 (short-dashed line), COS/G2 (dashed line), and COS/G3 (dotted line), along with the curves derived from experimental data obtained in 1986 (Ref. 118) (Exp1986: dotted-dashed line) and 2000 (Ref. 116) (Exp2000: solid line).

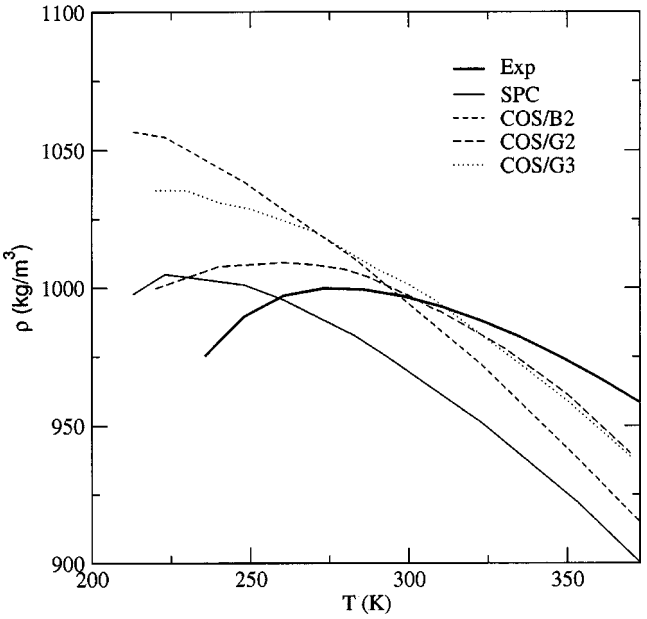

FIG. 8. Water density ρ at 1 atm as a function of temperature for the different water models. Experimental data (Ref. 119): thick line, SPC: solid line, COS/B2: short-dashed line, COS/G2: dashed line, and COS/G3: dotted line.

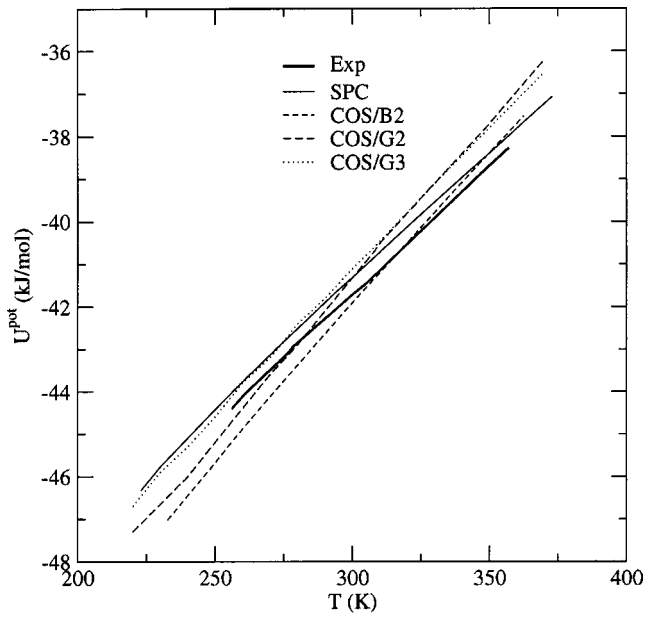

FIG. 9. Potential energy U^{pot} at 1 atm as a function of temperature for the different water models. Experimental data (Ref. 120): thick line, SPC: solid line, COS/B2: short-dashed line, COS/G2: dashed line, and COS/G3: dotted line.

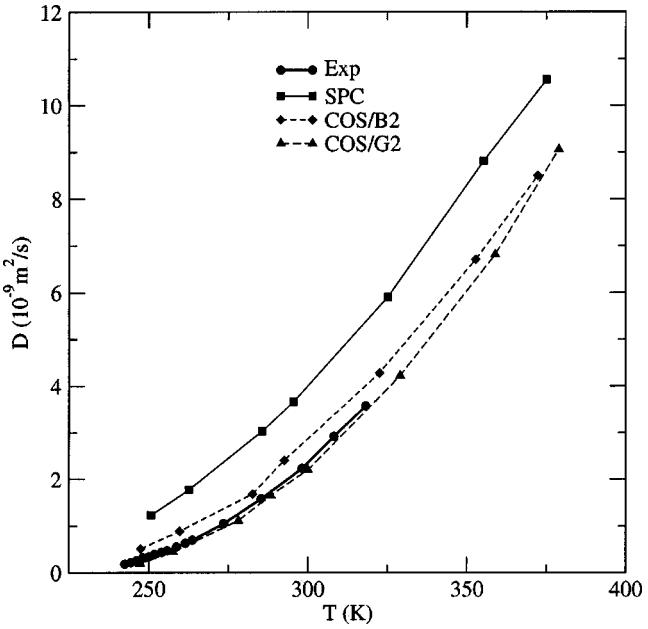

FIG. 10. Self-diffusion constant D at 1 atm as a function of temperature for the different water models. Experimental data (Refs. 122, 123): dots, SPC: squares, COS/B2: diamonds, and COS/G2: triangles.

erally, polarizable water models overestimate the heat capacity.[114] The isothermal compressibility κ_T is well reproduced while the thermal expansion coefficient α is overestimated by our models.

Sorenson *et al.*[115] provide a summary of experimental and simulated atom-atom RDF results obtained over many years. Two groups have now reported almost identical RDF curves based on independent analysis of neutron scattering experiments[116] or x-ray scattering experiments,[117] which represent the best RDF estimates currently available. Soper reported in 2000 (Ref. 116) a revised analysis of the experimental data obtained in 1986 (Ref. 118) (referred to as Exp2000 and Exp1986, respectively). The O-O, O-H, and H-H RDF $g(R)$ are shown in Fig. 7 for the COS/B2, COS/G2, COS/G3 models, and for the two experimental sets from Soper's group determined in 1986 (Ref. 118) and in 2000.[116] The data by Hura *et al.*[117] obtained with x rays is not shown since it is nearly indistinguishable from the Exp2000 data by Soper.[116] The first peak in the $g_{OO}(R)$ obtained from simulation is slightly overestimated compared to Exp2000, but comparable to Exp1986. The same is observed for the AMOEBA model.[59] The positions of the first peak for

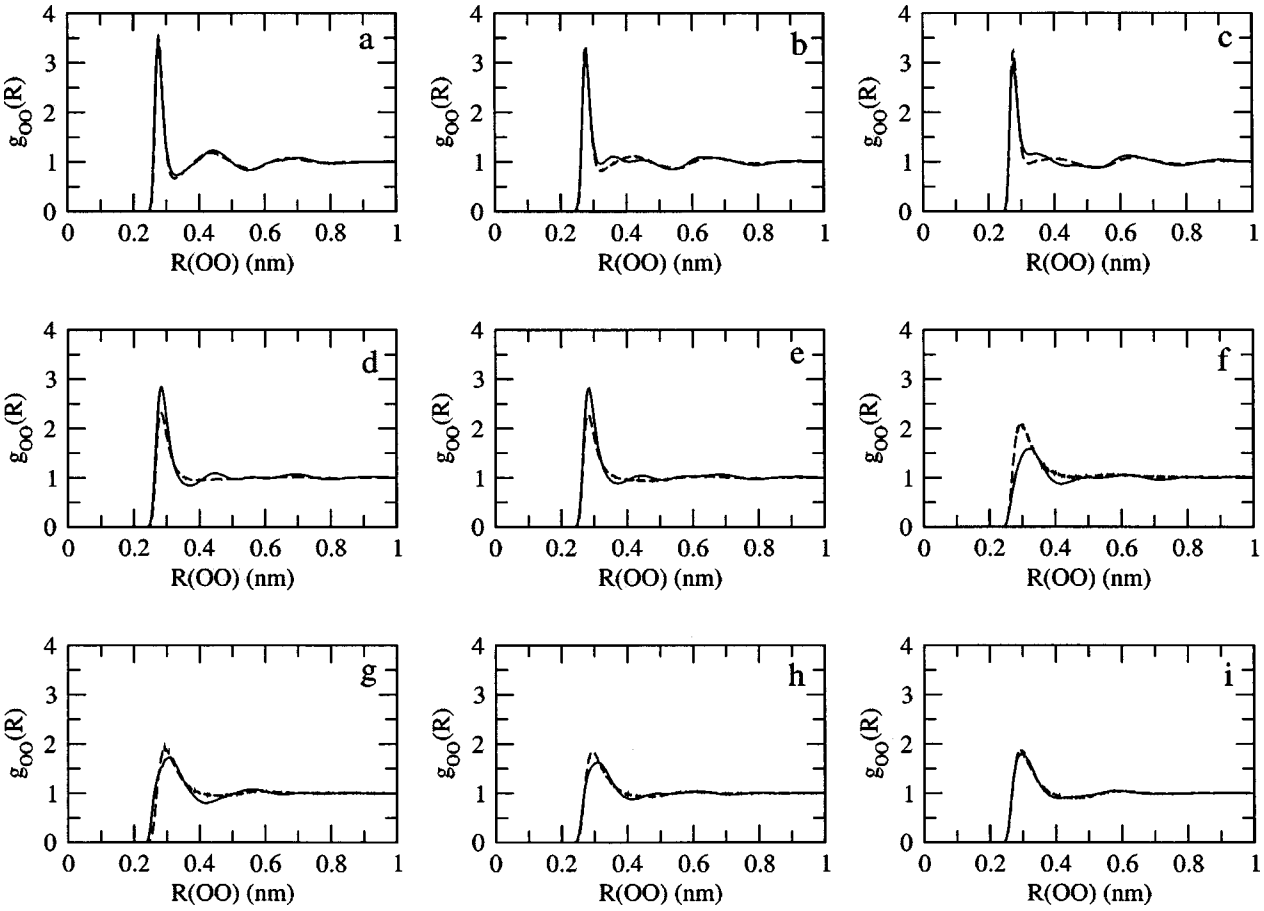

FIG. 11. Liquid phase oxygen-oxygen radial distribution functions at various thermodynamic states for the water model COS/G2 (dashed line) along with the curves derived from experimental data obtained in 2000 (Ref. 116) (Exp2000: solid line). (a) $T=268$ K, $P=270$ atm; (b) $T=268$ K, $P=2100$ atm; (c) $T=268$ K, $P=4000$ atm, (d) $T=423$ K, $P=100$ atm; (e) $T=423$ K, $P=1900$ atm; (f) $T=673$ K, $P=500$ atm; (g) $T=673$ K, $P=800$ atm; (h) $T=673$ K, $P=1300$ atm; (i) $T=673$ K, $P=3400$ atm.

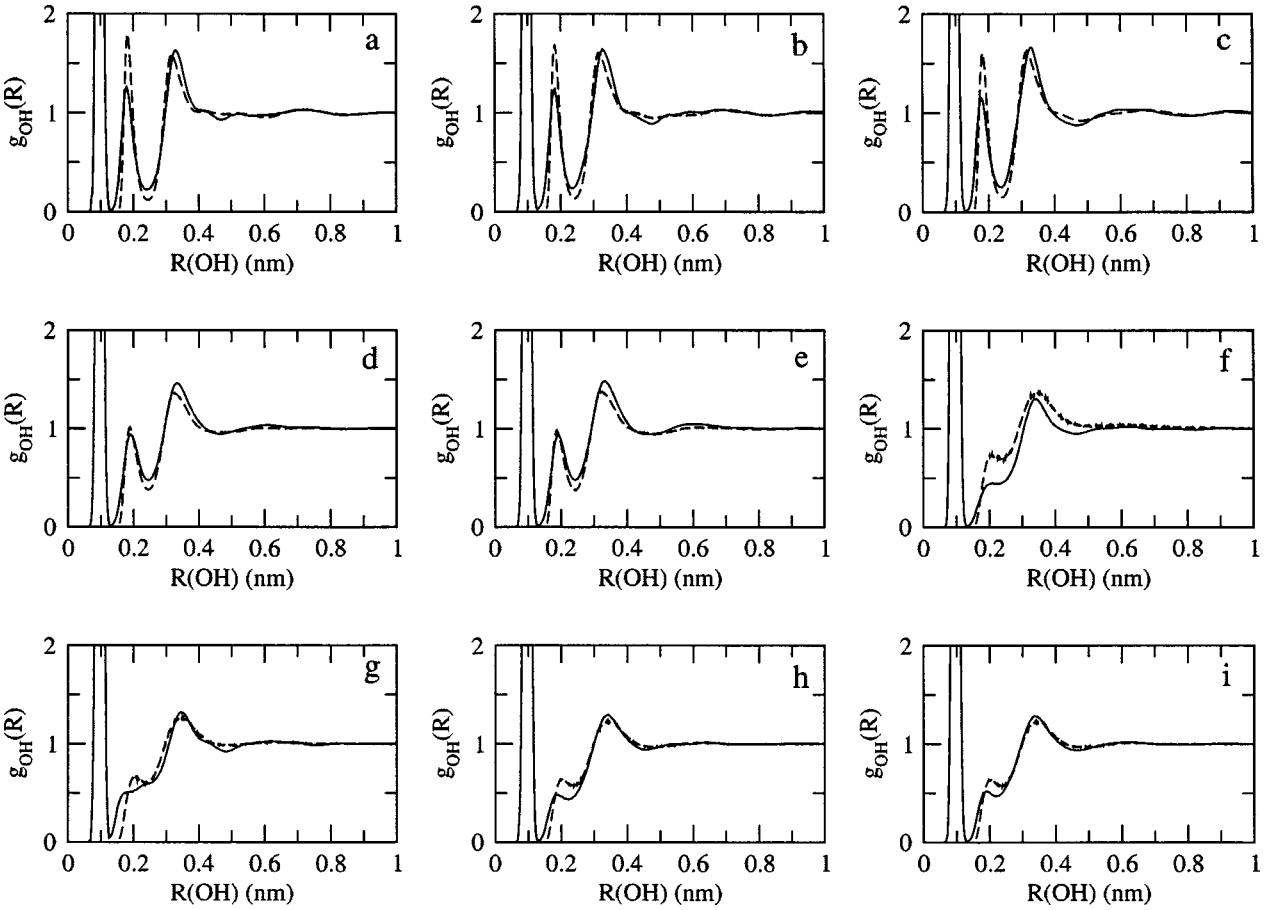

FIG. 12. Liquid phase oxygen-hydrogen radial distribution functions at various thermodynamic states for the water model COS/G2 (dashed line) along with the curves derived from experimental data obtained in 2000 (Ref. 116) (Exp2000: solid line). For further explanation see caption of Fig. 11.

the COS/G2 and COS/G3 models are 0.276 nm and 0.280 nm, lying between those of Exp1986 and Exp2000. The coordination number can be determined from the RDF by integrating $g_{OO}(R)$ over the first peak. Using the location of the first minimum on the experimental curve (0.336 nm)[116] as the upper limit of integration, we obtained a coordination number of 4.6, 4.6, 4.6, 4.5, and 4.5 for the COS/B2, COS/G2, COS/G3 models, Exp1986 and Exp2000, respectively. This shows that a water molecule is not strictly tetrahedrally coordinated. The COS/G2 model shows more structure in the second hydration shell than the COS/B2 model, while the COS/G3 model shows similar structure as the COS/B2 model. The first trough for the COS/G3 model is not deep enough and all the features are shifted out slightly too far. The simulated $g_{OH}(R)$ and $g_{HH}(R)$ agree with the experimental data.

C. Liquid water at nonambient temperatures and pressures

Densities as a function of temperature at 1 atm are compared with experimental data (taken from Ref. 119) in Fig. 8. As is well known, below a temperature of 4 °C, the density of cold water changes with temperature in a manner opposite to that of almost all other substances: with increasing temperature the tetrahedral structure breaks down and the density increases, leading to a maximum at about 4 °C. In our previous study,[25] the COS/B2 model did not show a density maximum above 200 K. The COS/G3 model shows similar behavior, which may be related to the fact that the O-O RDF for this model does not show a pronounced second peak.[16] The COS/G2 model, however, has a maximal density around 260 K. Generally, the densities of the models decrease too fast with increasing temperature compared to the experimental curve, which is also observed for other polarizable water models.

The potential energy U^{pot} as a function of temperature at 1 atm is shown in Fig. 9. Experimental data are derived from Ref. 120 with proper quantum corrections applied as done in Ref. 121. The computed potential energies vary linearly with temperature over a range of 150 K, which is consistent with the experimental data. For the polarizable models the potential energy increases too steeply with increasing temperature. This is reflected in the constant-pressure heat capacity C_p being too large.

We also calculated the self-diffusion constant as a function of temperature at 1 atm (Fig. 10). The two models (COS/G2 and COS/G3) show very similar curves and for clarity only that of the COS/G2 model is shown in Fig. 10. The polarizable water models reproduce better the experimental data.[122,123] A fit of the model results was made using the analytical function $D=D_0T^{1/2}[(T/T_s)-1]^{\gamma}$, which has been empirically shown to reproduce the isobaric tempera-

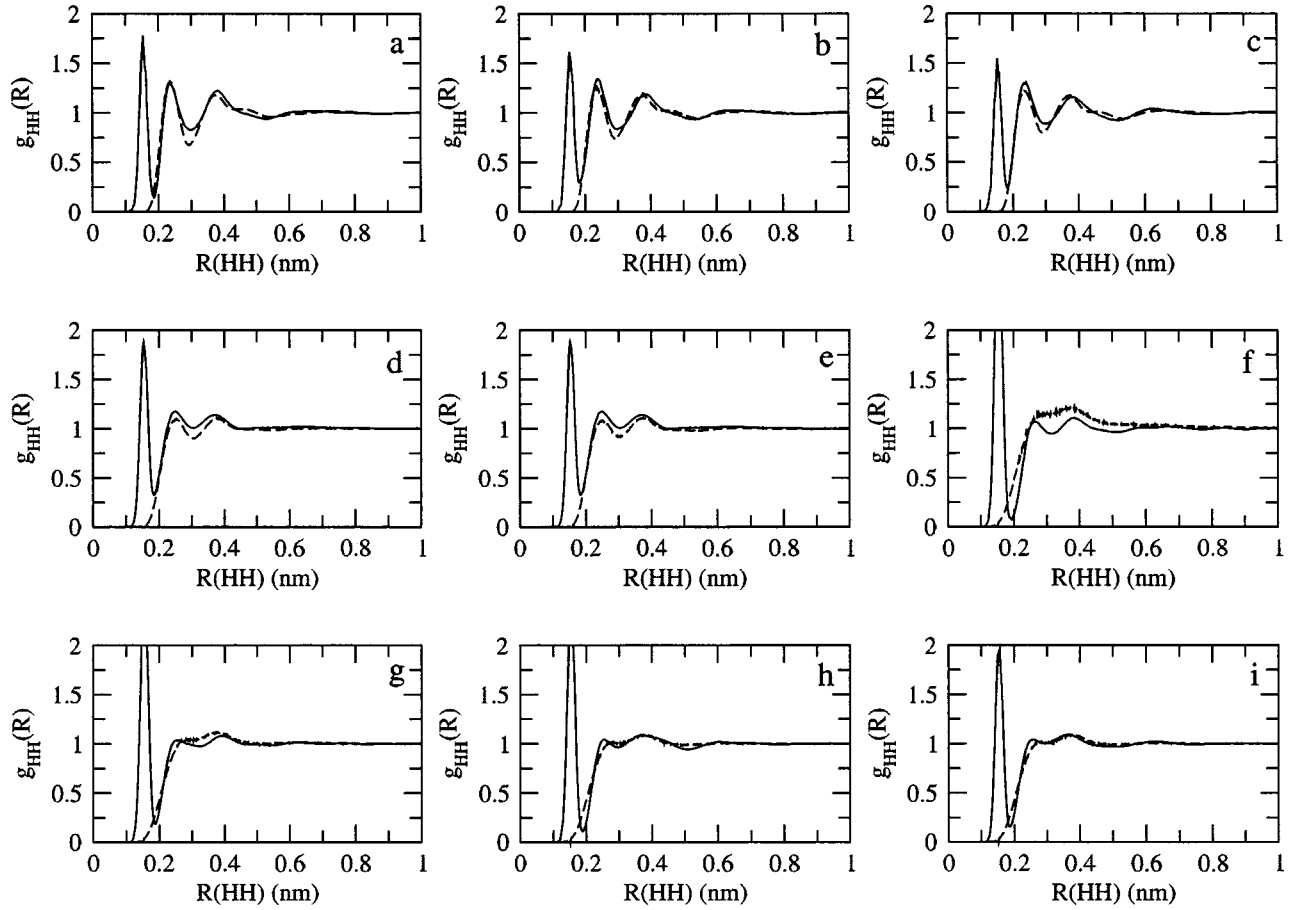

FIG. 13. Liquid phase hydrogen-hydrogen radial distribution functions at various thermodynamic states for the water model COS/G2 (dashed line) along with the curves derived from experimental data obtained in 2000 (Ref. 116) (Exp2000: solid line). For further explanation see caption of Fig. 11.

ture dependence of transport properties of liquid water.[124,125] The parameters from the fit for the COS/G2 model are $D_0 = 0.78 \times 10^{-9}\,\mathrm{m^2\,s^{-1}\,K^{-1/2}}$, $T_s = 218.9\,\mathrm{K}$, and $\gamma = 1.59$, comparable to the experimental ones $D_0 = 0.87 \times 10^{-9}\,\mathrm{m^2\,s^{-1}\,K^{-1/2}}$, $T_s = 220\,\mathrm{K}$, and $\gamma = 1.81$.

Atom-atom RDFs at several other thermodynamic conditions were computed for the COS/G2 and COS/G3 models and compared with the experimental data determined in 2000.[116] (For clarity, only those of the COS/G2 model are shown in Figs. 11–13). In general, the models agree well with experiment. Experimental evidence shows that the height of the first peak of $g_{OH}(R)$ decreases and its position shifts towards larger distances with increasing temperature and decreasing density.[116,118] This indicates a decrease of the number of hydrogen bonds and the model correctly captures this feature.

D. Ice

Molecular dynamics simulations of ice Ih form, the most common phase of ice, were performed at 100 K and 1 atm. The results are listed in Table V. The densities for ice at 100 K are 958.0 and 950.0 $\mathrm{kg\,m^{-3}}$, slightly larger than the experimental density of ice Ih at 100 K.[126] The lattice energy of the ice Ih form is computed as the energy required to infinitely separate the water molecules from the minimized ice geometry and is compared to the experimental value of $-47.34\ \mathrm{kJ\,mol^{-1}}$ at 0 K.[127] The oxygen-oxygen, oxygen-hydrogen, and hydrogen-hydrogen RDFs calculated from the final 100 ps of simulation are shown in Fig. 14 together with curves derived from experiments by Soper at 220 K.[116] RDFs calculated over different simulation periods show little changes (data not shown), which indicates a stable ice structure. Not unexpectedly, the RDFs derived from experiments at 220 K show less structure than those calculated from simulations at 100 K. However, both curves show the same features.

TABLE V. Properties of the COS/G2 and COS/G3 models in the solid state (ice Ih): density ρ, lattice energy U, average molecular dipole moment μ, and average induced dipole moment μ_{ind}. The experimental density ρ was determined at a temperature of 100 K (Ref. 126) and the lattice energy of ice Ih was determined at 0 K (Ref. 127).

Models	ρ ($\mathrm{kg\,m^{-3}}$)	μ (D)	μ_{ind} (D)	U ($\mathrm{kJ\,mol^{-1}}$)
COS/G2	958.0	2.81	0.97	−49.05
COS/G3	950.0	2.78	0.94	−48.52
Expt.	931.0[a]	2.6,[b] 3.09[c]		−47.34[d]
Ab initio		2.76,[c] 2.3–3.1[f]		

[a]Reference 126.
[b]Reference 91.
[c]Reference 103.
[d]Reference 127.
[c]Reference 137.
[f]Reference 107.

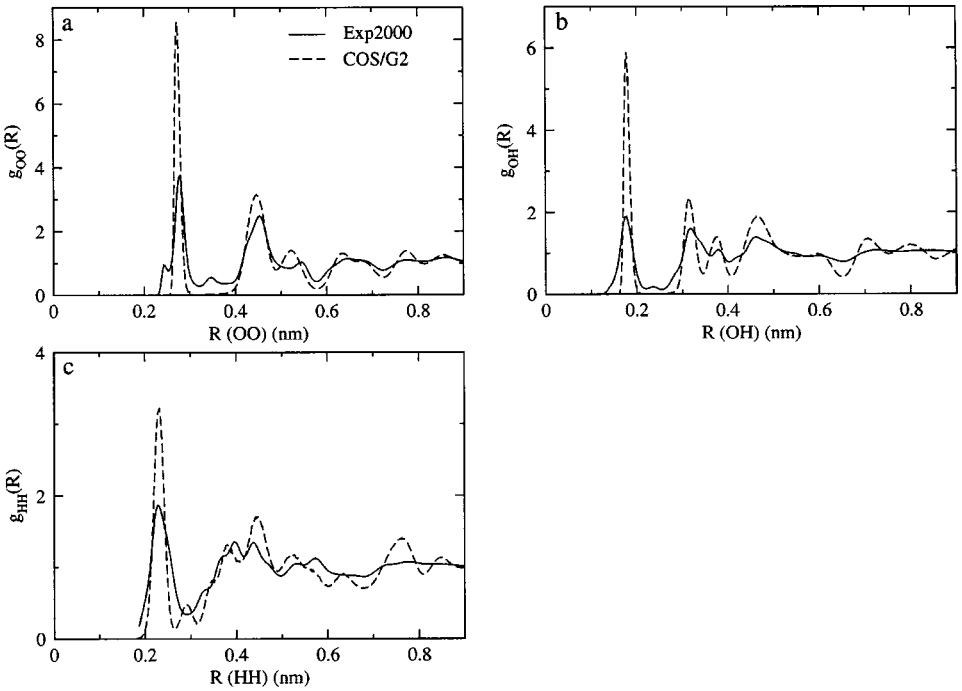

FIG. 14. Solid phase radial distribution functions for ice at 100 K for oxygen-oxygen (a), oxygen-hydrogen (b), hydrogen-hydrogen (c) atoms for the COS/G2 model calculated from the final 100 ps of simulation (dashed line) along with the curves derived from experimental data obtained at 220 K in 2000 (Ref. 116) (Exp2000: solid line).

IV. CONCLUSION

As pointed out before,[25] the COS type of model[35] circumvents the complex evaluation of dipole-dipole interactions and forces, and does not introduce any new type of interaction functions into the commonly used (bio)molecular force fields, since all the electrostatic interactions are point charge interactions. Thus a COS-type polarization model can very straightforwardly be combined with grid-based methods for evaluating the long-range electrostatic interactions and it is compatible with current biomolecular force fields.

In this paper, based on our previous work,[25] two new polarizable water models with a geometry of the SPC or TIP models were developed and validated through a series of MD simulations of water clusters, liquid water, and ice under various thermodynamic conditions. The main features of these two models include (1) one additional virtual atom site that was added to reproduce not only the gas phase dipole but also approximately the quadrupole moments of a water molecule, (2) no special damping factor parameters are needed to avoid short range overpolarization, and (3) the parameters of the models were fitted to reproduce the properties of liquid water at ambient conditions. The majority of the many-body effects is adequately accounted for by classical polarization in the two models. Compared to the previous COS/B2 model, both the COS/G2 and COS/G3 models improved the optimal dimer structure. We found that both the quadrupole moment and the out-of-plane polarizability play a crucial role in reproducing the gas phase properties. In the liquid phase at room temperature and pressure, the COS/G2 and COS/G3 models have a static dielectric permittivity of about 88 with an average dipole of 2.59 D and 2.57 D, respectively, which is a sizable improvement over the COS/B2 model.[25]

It has been argued that the inclusion of polarizability (together with flexibility and quantum effects) does not lead to a better reproduction of the thermodynamic properties of liquid water at a wide range of the thermodynamic state points.[75] However, many-body effects in water strongly depend on the molecular environment as shown in the calculations of water clusters (see Tables II and III). The polarization energy strongly varies with the cluster size. The average molecular dipole moment increases from the dimer to the large clusters, and the average molecular dipole moment of liquid water lies between those of various clusters. These features can only be captured by models that explicitly take into account polarization effects.

In the present work, only the linear approximation of the true polarization response to the electric field has been included.[24] It has been shown that in water, nonlinear polarization effects begin to become significant at a field strength of 2–3 V/Å,[128–130] which is comparable to the mean field strength in an aqueous solution.[45,108] Preliminary results from introducing high-order polarization effects into the COS/B2 model show some improvement in the properties of the liquid water.[131] On the other hand, introducing hyperpolarizability may complicate the model. Most water models have only a single repulsion-dispersion site (oxygen atom). Recent studies[18,59] show that the introduction of van der Waals interaction at the hydrogen atoms does improve the model properties. For simplicity, only one repulsion-dispersion center was considered in the present work.

In conclusion, we believe that both models will serve as reliable, simple, classical, rigid, polarizable water models in studying organic and (bio)molecular systems. Future work will include extending the models to ions, organic molecules, and nonpolar solvents and the use of the polarizable models to study ionic solutions, nonpolar solutes in polar solvents, polar solutes in nonpolar but polarizable solvents, and hydrogen-bonded liquids.

ACKNOWLEDGMENTS

Financial support was obtained from the Schweizer Nationalfonds, Project Number 2000-063590, which is gratefully acknowledged. We thank Dr. Alan Soper (Rutherford Appleton Laboratory, UK) for providing neutron scattering data of water, Dr. J. R. Reimers (University of Sydney, Australia) for providing the coordinates of the ice Ih unit cell, Professor Herman J. C. Berendsen (University of Groningen), Dr. Humberto Saint-Martin (Universidad Nacional Autónoma de México, México), Esra Neufeld (ETH Zürich), and Dr. Tomas Hansson (Karo Bio, Sweden) for helpful discussions.

[1] D. Eisenberg and W. Kauzmann, *The Structure and Properties of Water* (Clarendon Press, Oxford, 1969).
[2] A. Wallqvist and R. D. Mountain, in *Reviews in Computational Chemistry*, edited by K. B. Lipkowitz and D. B. Boyd (Wiley-VCH, New York, 1999), pp. 183–247.
[3] J. L. Finney, J. Mol. Liq. **90**, 303 (2001).
[4] B. Guillot, J. Mol. Liq. **101**, 219 (2002).
[5] J. W. Ponder and D. A. Case, Adv. Protein Chem. **66**, 27 (2003).
[6] W. D. Cornell, P. Cieplak, C. I. Bayly *et al*., J. Am. Chem. Soc. **117**, 5179 (1995).
[7] A. D. MacKerell, D. Bashford, M. Bellott *et al*., J. Phys. Chem. B **102**, 3586 (1998).
[8] W. F. van Gunsteren, S. R. Billeter, A. A. Eising, P. H. Hünenberger, P. Krüger, A. E. Mark, W. R. P. Scott, and I. G. Tironi, Biomolecular Simulation: The GROMOS Manual and User Guide (vdf Hochschulverlag, ETH Zürich, Switzerland, 1996).
[9] L. D. Schuler, X. Daura, and W. F. van Gunsteren, J. Comput. Chem. **22**, 1205 (2001).
[10] W. L. Jorgensen, D. S. Maxwell, and J. Tirado-Rives, J. Am. Chem. Soc. **118**, 11225 (1996).
[11] A. Rahman and F. H. Stillinger, J. Chem. Phys. **55**, 3336 (1971).
[12] H. J. C. Berendsen, J. P. M. Postma, W. F. van Gunsteren, and J. Hermans, in *Intermolecular forces*, edited by B. Pullman (Reidel, Dordrecht, 1981), pp. 331–342.
[13] W. L. Jorgensen, J. Chandrasekhar, J. D. Madura, R. W. Impey, and M. L. Klein, J. Chem. Phys. **79**, 926 (1983).
[14] H. J. C. Berendsen, J. R. Grigera, and T. P. Straatsma, J. Phys. Chem. **91**, 6269 (1987).
[15] M. Levitt, M. Hirshberg, R. Sharon, K. E. Laidig, and V. Daggett, J. Phys. Chem. B **101**, 5051 (1997).
[16] M. W. Mahoney and W. L. Jorgensen, J. Chem. Phys. **112**, 8910 (2000).
[17] M. W. Mahoney and W. L. Jorgensen, J. Chem. Phys. **114**, 363 (2001).
[18] A. Glättli, X. Daura, and W. F. van Gunsteren, J. Chem. Phys. **116**, 9811 (2002).
[19] A. Glättli, C. Oostenbrink, X. Daura, D. P. Geerke, H. B. Yu, and W. F. van Gunsteren, Braz. J. Phys. **34**, 116 (2004).
[20] A. Glättli, X. Daura, and W. F. van Gunsteren, J. Comput. Chem. **24**, 1087 (2003).
[21] S. A. Clough, Y. Beers, G. P. Klein, and L. S. Rothman, J. Chem. Phys. **59**, 2254 (1973).
[22] F. H. Stillinger, Science **209**, 451 (1980).
[23] T. A. Halgren and W. Damm, Curr. Opin. Struct. Biol. **11**, 236 (2001).
[24] S. W. Rick and S. J. Stuart, in *Reviews in Computational Chemistry*, edited by K. B. Lipowitz and D. B. Boyd (Wiley-VCH, New York, 2002), pp. 89–154.
[25] H. B. Yu, T. Hansson, and W. F. van Gunsteren, J. Chem. Phys. **118**, 221 (2003).
[26] F. J. Vesely, J. Comput. Phys. **24**, 361 (1977).
[27] F. H. Stillinger and C. W. David, J. Chem. Phys. **69**, 1473 (1978).
[28] P. Barnes, J. L. Finney, J. D. Nicholas, and J. E. Quinn, Nature (London) **282**, 459 (1979).
[29] A. Warshel, J. Phys. Chem. **83**, 1640 (1979).
[30] O. Matsuoka, E. Clementi, and M. Yoshimine, J. Chem. Phys. **64**, 1351 (1976).
[31] M. Sprik and M. L. Klein, J. Chem. Phys. **89**, 7556 (1988).
[32] J. A. C. Rullmann and P. T. van Duijnen, Mol. Phys. **63**, 451 (1988).
[33] P. Ahlström, A. Wallqvist, S. Engström, and B. Jönsson, Mol. Phys. **68**, 563 (1989).
[34] S. Kuwajima and A. Warshel, J. Phys. Chem. **94**, 460 (1990).
[35] T. P. Straatsma and J. A. McCammon, Mol. Simul. **5**, 181 (1990).
[36] J. Caldwell, L. X. Dang, and P. A. Kollman, J. Am. Chem. Soc. **112**, 9144 (1990).
[37] U. Niesar, G. Corongiu, E. Clementi, G. R. Kneller, and D. K. Bhattacharya, J. Phys. Chem. **94**, 7949 (1990).
[38] S. B. Zhu, S. Singh, and G. W. Robinson, J. Chem. Phys. **95**, 2791 (1991).
[39] A. K. Rappé and W. A. Goddard, J. Phys. Chem. **95**, 3358 (1991).
[40] L. X. Dang, J. Chem. Phys. **97**, 2659 (1992).
[41] D. N. Bernardo, Y. B. Ding, K. Kroghjespersen, and R. M. Levy, J. Phys. Chem. **98**, 4180 (1994).
[42] S. W. Rick, S. J. Stuart, and B. J. Berne, J. Chem. Phys. **101**, 6141 (1994).
[43] J. Brodholt, M. Sampoli, and R. Vallauri, Mol. Phys. **86**, 149 (1995).
[44] J. W. Caldwell and P. A. Kollman, J. Phys. Chem. **99**, 6208 (1995).
[45] I. M. Svishchev, P. G. Kusalik, J. Wang, and R. J. Boyd, J. Chem. Phys. **105**, 4742 (1996).
[46] A. A. Chialvo and P. T. Cummings, J. Chem. Phys. **105**, 8274 (1996).
[47] L. X. Dang and T. M. Chang, J. Chem. Phys. **106**, 8149 (1997).
[48] S. Brdarski and G. Karlström, J. Phys. Chem. A **102**, 8182 (1998).
[49] H. A. Stern, G. A. Kaminski, J. L. Banks, R. H. Zhou, B. J. Berne, and R. A. Friesner, J. Phys. Chem. B **103**, 4730 (1999).
[50] C. J. Burnham, J. C. Li, S. S. Xantheas, and M. Leslie, J. Chem. Phys. **110**, 4566 (1999).
[51] B. Chen, J. H. Xing, and J. I. Siepmann, J. Phys. Chem. B **104**, 2391 (2000).
[52] S. W. Rick, J. Chem. Phys. **114**, 2276 (2001).
[53] H. A. Stern, F. Rittner, B. J. Berne, and R. A. Friesner, J. Chem. Phys. **115**, 2237 (2001).
[54] B. Guillot and Y. Guissani, J. Chem. Phys. **114**, 6720 (2001).
[55] P. J. van Maaren and D. van der Spoel, J. Phys. Chem. B **105**, 2618 (2001).
[56] S. Iuchi, A. Morita, and S. Kato, J. Phys. Chem. B **106**, 3466 (2002).
[57] C. J. Burnham and S. S. Xantheas, J. Chem. Phys. **116**, 1500 (2002).
[58] C. J. Burnham and S. S. Xantheas, J. Chem. Phys. **116**, 5115 (2002).
[59] P. Y. Ren and J. W. Ponder, J. Phys. Chem. B **107**, 5933 (2003).
[60] G. Lamoureux, A. D. MacKerell, and B. Roux, J. Chem. Phys. **119**, 5185 (2003).
[61] G. Lamoureux and B. Roux, J. Chem. Phys. **119**, 3025 (2003).
[62] E. Lussetti, G. Pastore, and E. Smargiassi, Chem. Phys. Lett. **381**, 287 (2003).
[63] W. F. Murphy, J. Chem. Phys. **67**, 5877 (1977).
[64] P. Drude, *The Theory of Optics* (Longmans, Green, New York, 1902).
[65] M. Born and K. Huang, *Dynamic Theory of Crystal Lattices* (Oxford University Press, Oxford, UK, 1954).
[66] M. Neumann, Mol. Phys. **50**, 841 (1983).
[67] R. W. Hockney and J. W. Eastwood, *Computer Simulation Using Particles*, 2nd ed. (Institute of Physics Publishing, Bristol, UK, 1988).
[68] I. G. Tironi, R. Sperb, P. E. Smith, and W. F. van Gunsteren, J. Chem. Phys. **102**, 5451 (1995).
[69] B. A. Luty and W. F. van Gunsteren, J. Phys. Chem. **100**, 2581 (1996).
[70] P. H. Hünenberger, in *Simulation and Theory of Electrostatic Interactions in Solution: Computational Chemistry, Biophysics, and Aqueous Solutions*, edited by L. Pratt and G. Hummer (American Institute of Physics, New York, USA, 1999), pp. 17–83.
[71] P. H. Hünenberger, J. Chem. Phys. **116**, 6880 (2002).
[72] B. Oliva and P. H. Hünenberger, J. Chem. Phys. **116**, 6898 (2002).
[73] I. G. Tironi, R. M. Brunne, and W. F. van Gunsteren, Chem. Phys. Lett. **250**, 19 (1996).
[74] J. Zhou, S. Reich, and B. R. Brooks, J. Chem. Phys. **112**, 7919 (2000).
[75] M. W. Mahoney and W. L. Jorgensen, J. Chem. Phys. **115**, 10758 (2001).
[76] B. Hess, H. Saint-Martin, and H. J. C. Berendsen, J. Chem. Phys. **116**, 9602 (2002).
[77] M. Christen and W. F. van Gunsteren, J. Chem. Phys. (to be published).
[78] S. Y. Liem, P. L. A. Popelier, and M. Leslie, Int. J. Quantum Chem. **99**, 685 (2004).
[79] H. J. C. Berendsen and W. F. van Gunsteren, in *Molecular Liquids-Dynamics and Interactions*, edited by A. J. Barnes, W. J. Orville-Thomas, and J. Yarwood (Reidel, Dordrecht, 1984), pp. 475–500.
[80] G. A. Kaminski, H. A. Stern, B. J. Berne, and R. A. Friesner, J. Phys. Chem. A **108**, 621 (2004).
[81] X. Daura, A. E. Mark, and W. F. van Gunsteren, J. Comput. Chem. **19**, 535 (1998).

[82] C. Oostenbrink, A. Villa, A. E. Mark, and W. F. van Gunsteren, J. Comput. Chem. **25**, 1656 (2004).
[83] A. Morita and S. Kato, J. Chem. Phys. **110**, 11987 (1999).
[84] A. Morita, J. Comput. Chem. **23**, 1466 (2002).
[85] G. S. Kell, J. Chem. Eng. Data **12**, 66 (1967).
[86] W. R. P. Scott, P. H. Hünenberger, I. G. Tironi *et al*., J. Phys. Chem. A **103**, 3596 (1999).
[87] J.-P. Ryckaert, G. Ciccotti, and H. J. C. Berendsen, J. Comput. Phys. **23**, 327 (1977).
[88] H. J. C. Berendsen, J. P. M. Postma, W. F. van Gunsteren, A. Di Nola, and J. R. Haak, J. Chem. Phys. **81**, 3684 (1984).
[89] J. A. Hayward and J. R. Reimers, J. Chem. Phys. **106**, 1518 (1997).
[90] W. Klopper, J. G. C. M. van Duijneveldt-van de Rijdt, and F. B. van Duijneveldt, Phys. Chem. Chem. Phys. **2**, 2227 (2000).
[91] C. A. Coulson and D. Eisenberg, Proc. R. Soc. London, Ser. A **291**, 445 (1966).
[92] P. A. Kollman, Acc. Chem. Res. **10**, 365 (1977).
[93] M. Alfredsson, J. P. Brodholt, K. Hermanson, and R. Vallauri, Mol. Phys. **94**, 873 (1998).
[94] B. T. Thole, Chem. Phys. **59**, 341 (1981).
[95] M. J. Frisch, G. W. Trucks, H. B. Schlegel *et al*., GAUSSIAN 98, Revision A.11.1 Gaussian, Inc., Pittsburgh, PA, 2001.
[96] S. S. Xantheas, C. J. Burnham, and R. J. Harrison, J. Chem. Phys. **116**, 1493 (2002).
[97] F. N. Keutsch and R. J. Saykally, Proc. Natl. Acad. Sci. U.S.A. **98**, 10533 (2001).
[98] F. N. Keutsch, J. D. Cruzan, and R. J. Saykally, Chem. Rev. (Washington, D.C.) **103**, 2533 (2003).
[99] K. Watanabe and M. L. Klein, Chem. Phys. **131**, 157 (1989).
[100] R. C. Weast, *Handbook of Chemistry and Physics* (CRC, Boca Raton, 1983).
[101] M. Sprik, J. Chem. Phys. **95**, 6762 (1991).
[102] P. L. Silvestrelli and M. Parrinello, J. Chem. Phys. **111**, 3572 (1999).
[103] E. R. Batista, S. S. Xantheas, and H. Jönsson, J. Chem. Phys. **109**, 4546 (1998).
[104] E. R. Batista, S. S. Xantheas, and H. Jönsson, J. Chem. Phys. **112**, 3285 (2000).
[105] K. Laasonen, M. Sprik, M. Parrinello, and R. Car, J. Chem. Phys. **99**, 9080 (1993).
[106] A. V. Gubskaya and P. G. Kusalik, J. Chem. Phys. **117**, 5290 (2002).
[107] E. R. Batista, S. S. Xantheas, and H. Jönsson, J. Chem. Phys. **111**, 6011 (1999).
[108] Y. S. Badyal, M. L. Saboungi, D. L. Price, S. D. Shastri, D. R. Haeffner, and A. K. Soper, J. Chem. Phys. **112**, 9206 (2000).
[109] J. C. Soetens, M. T. C. M. Costa, and C. Millot, Mol. Phys. **94**, 577 (1998).
[110] S. Chalmet and M. F. Ruiz-Lopez, J. Chem. Phys. **115**, 5220 (2001).
[111] A. D. Buckingham, Proc. R. Soc. London, Ser. A **238**, 235 (1956).
[112] U. Kaatze, J. Chem. Eng. Data **34**, 371 (1989).
[113] M. P. Allen and D. J. Tildesley, *Computer Simulation of Liquids* (Oxford University Press, Oxford, UK, 1987).
[114] P. Jedlovszky and J. Richardi, J. Chem. Phys. **110**, 8019 (1999).
[115] J. M. Sorenson, G. Hura, R. M. Glaeser, and T. Head-Gordon, J. Chem. Phys. **113**, 9149 (2000).
[116] A. K. Soper, Chem. Phys. **258**, 121 (2000).
[117] G. Hura, J. M. Sorenson, R. M. Glaeser, and T. Head-Gordon, J. Chem. Phys. **113**, 9140 (2000).
[118] A. K. Soper and M. G. Phillips, Chem. Phys. **107**, 47 (1986).
[119] G. S. Kell, J. Chem. Eng. Data **20**, 97 (1975).
[120] J. A. Riddick, W. B. Bunger, and T. K. Sakano, *Organic Solvents: Physical Properties and Methods of Purification* (Wiley, New York, 1986).
[121] J. P. M. Postma, Ph.D. thesis, Rijksuniversiteit, Groningen, The Netherlands, 1985.
[122] K. T. Gillen, D. C. Douglass, and J. R. Hoch, J. Chem. Phys. **57**, 5117 (1972).
[123] R. Mills, J. Phys. Chem. **77**, 685 (1973).
[124] F. X. Prielmeier, E. W. Lang, R. J. Speedy, and H. D. Ludemann, Phys. Rev. Lett. **59**, 1128 (1987).
[125] R. J. Speedy and C. A. Angell, J. Chem. Phys. **65**, 851 (1976).
[126] K. Rottger, A. Endriss, J. Ihringer, S. Doyle, and W. F. Kuhs, Acta Crystallogr., Sect. B: Struct. Sci. **50**, 644 (1994).
[127] E. Whalley, J. Chem. Phys. **81**, 4087 (1984).
[128] P. Kaatz, E. A. Donley, and D. P. Shelton, J. Chem. Phys. **108**, 849 (1998).
[129] G. Maroulis, J. Chem. Phys. **94**, 1182 (1991).
[130] G. Maroulis, Chem. Phys. Lett. **289**, 403 (1998).
[131] E. Neufeld, H. B. Yu, T. Hansson, and W. F. van Gunsteren (unpublished).
[132] L. A. Curtiss, D. J. Frurip, and M. Blander, J. Chem. Phys. **71**, 2703 (1979).
[133] J. A. Odutola and T. R. Dyke, J. Chem. Phys. **72**, 5062 (1980).
[134] J. Hasted, in *Water, A Comprehensive Treatise*, edited by F. Franks (Plenum, New York, 1972), pp. 255–309.
[135] K. Ichikawa, Y. Kameda, T. Yamaguchi, H. Wakita, and M. Misawa, Mol. Phys. **73**, 79 (1991).
[136] J. Verhoeve and A. Dymanus, J. Chem. Phys. **52**, 3222 (1970).
[137] J. K. Gregory, D. C. Clary, K. Liu, M. G. Brown, and R. J. Saykally, Science **275**, 814 (1997).
[138] H. M. Lee, S. B. Suh, J. Y. Lee, P. Tarakeshwar, and K. S. Kim, J. Chem. Phys. **112**, 9759 (2000).
[139] H. Saint-Martin, J. Hernandez-Cobos, M. I. Bernal-Uruchurtu, I. Ortega-Blake, and H. J. C. Berendsen, J. Chem. Phys. **113**, 10899 (2000).
[140] J. E. Fowler and H. F. Schaefer, J. Am. Chem. Soc. **117**, 446 (1995).
[141] S. S. Xantheas and T. H. Dunning, J. Chem. Phys. **99**, 8774 (1993).
[142] M. P. Hodges, A. J. Stone, and S. S. Xantheas, J. Phys. Chem. A **101**, 9163 (1997).
[143] I. M. B. Nielsen, E. T. Seidl, and C. L. Janssen, J. Chem. Phys. **110**, 9435 (1999).
[144] N. Pugliano and R. J. Saykally, Science **257**, 1937 (1992).
[145] J. D. Cruzan, M. R. Viant, M. G. Brown, and R. J. Saykally, J. Phys. Chem. A **101**, 9022 (1997).
[146] K. Liu, M. G. Brown, and R. J. Saykally, J. Phys. Chem. A **101**, 8995 (1997).
[147] J. Kim and K. S. Kim, J. Chem. Phys. **109**, 5886 (1998).
[148] K. Krynicki, C. D. Green, and D. W. Sawyer, Faraday Discuss. **66**, 199 (1978).
[149] B. Halle and H. Wennerström, J. Chem. Phys. **75**, 1928 (1981).
[150] R. Ludwig, Chem. Phys. **195**, 329 (1995).
[151] K. Krynicki, Physica (Amsterdam) **32**, 167 (1966).
[152] M. Neumann, Mol. Phys. **57**, 97 (1986).